

Microglia phenotypes are associated with subregional patterns of concomitant tau, amyloid- β and α -synuclein pathologies in the hippocampus of patients with Alzheimer's disease and dementia with Lewy bodies

Journal Article**Author(s):**

Fixemer, Sonja; Ameli, Corrado; Hammer, Gaël; Salamanca, Luis; Uriarte Huarte, Oihane; Schwartz, Chantal; Gérardy, Jean-Jacques; Mechawar, Naguib; Skupin, Alexander; Mittelbronn, Michel; Bouvier, David S.

Publication date:

2022-03-16

Permanent link:

<https://doi.org/10.3929/ethz-b-000539239>

Rights / license:

[Creative Commons Attribution 4.0 International](#)

Originally published in:


Acta Neuropathologica Communications 10, <https://doi.org/10.1186/s40478-022-01342-7>

RESEARCH

Open Access



Microglia phenotypes are associated with subregional patterns of concomitant tau, amyloid- β and α -synuclein pathologies in the hippocampus of patients with Alzheimer's disease and dementia with Lewy bodies

Sonja Fixemer^{1,2†}, Corrado Ameli^{1†}, Gaël Hammer^{2,3}, Luis Salamanca^{1,4}, Oihane Uriarte Huarte^{1,2}, Chantal Schwartz³, Jean-Jacques Gérardy^{2,3}, Naguib Mechawar⁵, Alexander Skupin¹, Michel Mittelbronn^{1,2,3,6,7,8} and David S. Bouvier^{1,2,3*} 

Abstract

The cellular alterations of the hippocampus lead to memory decline, a shared symptom between Alzheimer's disease (AD) and dementia with Lewy Bodies (DLB) patients. However, the subregional deterioration pattern of the hippocampus differs between AD and DLB with the CA1 subfield being more severely affected in AD. The activation of microglia, the brain immune cells, could play a role in its selective volume loss. How subregional microglia populations vary within AD or DLB and across these conditions remains poorly understood. Furthermore, how the nature of the hippocampal local pathological imprint is associated with microglia responses needs to be elucidated. To this purpose, we employed an automated pipeline for analysis of 3D confocal microscopy images to assess CA1, CA3 and DG/CA4 subfields microglia responses in post-mortem hippocampal samples from late-onset AD ($n = 10$), DLB ($n = 8$) and age-matched control (CTL) ($n = 11$) individuals. In parallel, we performed volumetric analyses of hyperphosphorylated tau (pTau), amyloid- β (A β) and phosphorylated α -synuclein (pSyn) loads. For each of the 32,447 extracted microglia, 16 morphological features were measured to classify them into seven distinct morphological clusters. Our results show similar alterations of microglial morphological features and clusters in AD and DLB, but with more prominent changes in AD. We identified two distinct microglia clusters enriched in disease conditions and particularly increased in CA1 and DG/CA4 of AD and CA3 of DLB. Our study confirms frequent concomitance of pTau, A β and pSyn loads across AD and DLB but reveals a specific subregional pattern for each type of pathology, along with a generally increased severity in AD. Furthermore, pTau and pSyn loads were highly correlated across subregions and conditions. We uncovered tight associations between microglial changes and the subfield pathological imprint. Our findings suggest that combinations and severity of subregional pTau, A β and pSyn pathologies transform local microglia phenotypic composition in the hippocampus. The high burdens of pTau and pSyn associated with increased microglial alterations could be a factor in CA1 vulnerability in AD.

*Correspondence: David.Bouvier@lns.etat.lu

[†]Sonja Fixemer and Corrado Ameli contributed equally to this work.

³Laboratoire National de Santé (LNS), National Center of Pathology (NCP), Dudelange, Luxembourg

Full list of author information is available at the end of the article



Keywords: Alzheimer's disease, Dementia with Lewy Bodies, Hippocampus, Microglia, Amyloid- β , Hyperphosphorylated tau, Phosphorylated α -synuclein

Introduction

The decline of memory is a shared symptom in age-related neurodegenerative diseases [24]. The atrophy of the hippocampus, essential for memory formation and consolidation [9, 13, 49], is associated with memory impairment in normal ageing [34] and is predictive of Alzheimer's disease (AD) and associated dementia [3, 26]. The hippocampus is one of the most severely affected brain regions in AD and dementia with Lewy Bodies (DLB) [4, 20, 28, 64] but the causes of its vulnerability are still poorly understood. The hippocampal architecture has been widely studied for its tri-synaptic loop circuitry and its composition in five distinct subfields, the *dentate gyrus* (DG), as well as the four *Cornu ammonis* (CA) fields [8] dedicated to specific types or sequences of memory processes [18, 82, 94]. The subregional pattern of atrophy of the hippocampus in AD is distinct from other groups of neurodegenerative conditions. The severe loss of volume in CA1 serves as an anatomical correlate in imaging to classify patients, CA1 being more preserved in patients with DLB compared to AD [1, 3, 40, 43, 53, 74, 96]. Understanding the molecular and cellular mechanisms that lead to such a subregional vulnerability in the AD hippocampus compared to a milder and more homogenous deterioration in DLB could unveil personalized therapeutic strategies to alleviate the progression of memory decline.

Microglia, the innate immune cells of the CNS, regulate homeostasis by clearing pathogens, cell debris and dying cells [55]. Microglia are constantly surveying their micro-environment with their moving ramifications and react quickly to insults by adopting an activated profile associated with a decrease of branches and an amoeboid form [79]. They are involved in numerous responses such as the secretion of anti- and pro-inflammatory molecules, and phagocytosis, that could be protective or detrimental by accelerating neuronal deterioration depending on the context [78]. Genome-wide association studies (GWAS) identified AD onset risk loci that are associated with genes involved in microglia physiology and responses, such as *CRI* (complement receptor type 1), *SPI1* (transcription factor PU.1), *TREM2* (triggering receptor expressed on myeloid cells 2) and *CD33* [61]. New technologies such as single cell RNA-sequencing, have redefined the roles and phenotypes of microglia in brain disorders and unveiled a complex regional and temporal heterogeneity of their signatures across mouse models and neurodegenerative conditions in human [7,

56, 69, 76, 90]. PET imaging correlated microglia activation with hippocampal volume loss [25] but if and how microglia play a role in the subregional deterioration pattern of AD is poorly understood. Furthermore, some studies have shown differences in microglia responses between AD and DLB [2, 6, 16, 52, 86, 87], DLB microglia seemingly less altered and responsive in numerous brain regions. How their subregional responses within the hippocampus differ from AD remains unclear. Additionally, microglia responses have been associated with misfolded protein pathologies in cell cultures and monogenic rodent models [36, 48, 51, 67, 77, 83, 95] but AD and DLB samples often show overlapping pathologies, extracellular senile plaques made of amyloid- β ($A\beta$) peptides, intracellular neurofibrillary tangles (NFTs) built from hyperphosphorylated tau (pTau) and intracellular aggregation of phosphorylated α -synuclein (pSyn) such as Lewy bodies [47], with different gradients of severity [12, 59, 60, 88]. The association between microglia phenotypes and mixed-pathological contexts still needs to be clarified.

In this study, we have investigated how microglia responses differ in AD and DLB cases across the CA1, CA3 and DG/CA4 subfields of the hippocampus and their relationship with pTau, $A\beta$ and pSyn pathologies patterns. To this purpose, we immunostained thick and consecutive sections with Iba1, pTau, $A\beta$, or pSyn antibodies and employed high-content 3D confocal microscopy combined with image analysis tools such as our Microglia and Immune Cells Morphologies Analyser and Classifier (MIC-MAC) pipeline [75] on a collection of neuropathologically diagnosed post-mortem AD and DLB cases, and age-matched control (CTL) samples. Our approach allowed a very detailed and 3D understanding of microglia changes at the individual level in the various subfields of the hippocampus and highlighted their local association with concomitant pTau, $A\beta$ and pSyn loads. We report for the first time the relation between the remodelling of local microglia population and the subregional pattern, the co-occurrence and severity of pTau, $A\beta$ and pSyn pathologies across AD and DLB.

Materials and methods

Human brain samples and processing

All experiments involving human tissues were conducted in accordance with the guidelines approved by the Ethics Board of the Douglas Bell Canada Brain Bank (Douglas Mental Health University Institute, Montréal, QC,

Canada) and the Ethic Panel of the University of Luxembourg (ERP 16-037 and 21-009). All pseudonymized autopsy brain samples were provided by the Douglas Bell Canada Brain Bank (formalin samples) and the Luxembourg Brain Bank (formalin-fixed paraffin-embedded (FFPE) samples) (see Table 1). Hippocampal samples (median part of the hippocampus, between the uncus and *corpus geniculatum laterale*) were dissected from cases of neuropathologically confirmed AD and DLB, as well as from age-matched CTLs. Samples were evaluated regarding A β plaques, NFTs and α -synuclein and

assessed according to Braak, ABC staging [12, 63] and Mc Keith staging criteria [59] by an affiliated neuropathologist of the Douglas Bell Canada Brain Bank. This study comprises age-matched CTLs with no history of dementia. However, some CTL cases showed low levels of neuropathological abnormalities such as AD pathology. Brain samples used for the volumetric study were preserved in 10% formalin until processing as indicated in Table 1.

Table 1 Demographic and neuropathological data of human samples

Diagnosis	Case	Sex	Age (years)	PMD (hours)	Disease score	Reported concomitant misfolded protein pathologies*
<i>CTL</i>						
	1	F	86	5.7	/	/
	2	F	80	17.5	/	/
	3	F	89	23.6	/	Some senile plaques and NFTs
	4	M	89	32.2	/	/
	5	M	80	13.0	/	Some senile plaques
	6	F	83	35.7	/	/
	7	F	95	23.7	/	/
	8	M	85	26.7	/	/
	9	M	83	16.8	/	/
	10	M	89	31.9	/	A1B1C1
	11	F	55	21.1	/	/
<i>DLB</i>						
	12	M	70	24.5	Neo-cortical diffuse	Senile plaques and NFTs
	13	M	89	17.0	Limbic transitional	Mixed AD
	14	M	75	21.0	Neo-cortical	Senile plaques and NFTs
	15	M	64	17.2	Neo-cortical	Senile plaques and NFTs
	16	F	83	17.7	Neo-cortical	Senile plaques and NFTs
	17	M	82	22.0	Neo-cortical diffuse	/
	18	F	81	8.6	Neo-cortical diffuse	/
	19	F	74	27.6	Neo-cortical	A2B2C0
	20	M	91	85.0	Neo-cortical diffuse	Braak III/IV
<i>AD</i>						
	21	M	80	15.5	Braak IV	/
	22	M	82	11.5	Braak IV	/
	23	M	85	31.1	A2B3C2	/
	24	F	83	25.0	A2B3C2	/
	25	M	91	25.0	A2B3C2	/
	26	F	96	26.5	Braak IV/V	/
	27	M	87	21.7	A2B3C2	/
	28	M	90	26.1	A3B2C3	/
	29	F	87	17.0	A1B2C2	/
	30	M	90	32.0	A2B2C3	/

AD Alzheimer's disease, CTLs age-matched controls, DLB Dementia with Lewy Bodies, NFTs neurofibrillary tangles, PMD post-mortem delay

*After neuropathological examination

Post-mortem case description

The description of the samples is detailed in Table 1. We ran our image-based analysis on age-matched CTLs ($n=11$), with no or low levels of neuropathological alterations as well as on neuropathologically confirmed AD (A1B2C2 to severe stages A2B3C2 or Braak IV) ($n=10$) and DLB (limbic transitional to neocortical diffuse) ($n=8$) cases often bearing a certain amount of AD pathologies. The median age at death and average post-mortem delay (PMD) did not differ significantly between groups and are 83.1 years and 22.6 h for CTLs; 87.1 years and 23.1 h for AD; and 77.3 years and 19.4 h for DLB. Sex representation is slightly unbalanced with female cases being respectively 54.5% for CTLs, 30% for AD and 37.5% for DLB. Average time spent in fixative was also approximately similar for specimens of all groups (CTLs, 14.7 years; AD, 11.1 years and DLB, 12.2 years).

Immunohistochemistry

The FFPE sample from the Luxembourg Brain Bank was used to validate pSyn, 4G8 and AT8 antibodies on 3 μm sections. Briefly, sections were processed by an automated immunostainer (Omnis Immunostainer, Agilent, Glostrup, Denmark) with primary antibodies 4G8, AT8 or against PS129-synuclein. For all three primary antibodies, heat retrieval was performed with the Envision Flex Tris low pH buffer (Agilent) for 30 min at 97 °C on board, primary antibodies were incubated 20 min at room temperature (RT), and detection was performed with the Envision Flex Detection kit (Agilent) based on the DAB/HRP substrate system. The sections were counterstained with hematoxylin.

The formalin hippocampal samples were washed in phosphate buffer saline (PBS), cryo-preserved in 30% sucrose in PBS for 36 h approximately and embedded in an M-1 embedding matrix (Thermo scientific, USA). Then, they were cut into 80 to 100 μm thick slices on a sliding freezing microtome (LeicaSM2010R) and

preserved at -20 °C in a cryoprotectant solution [Ethylene glycol (30%), and glycerol (30%) in 0.05 M phosphate buffer (PB, pH 7.4)]. Immunostainings were performed as previously described [10, 70] without antigen retrieval. In brief, after an overnight UV irradiation (UV lamp Ushio, 30 Watt) which reduces the autofluorescence of the human fixed samples [10, 70] sections were permeabilized for 30 min with 0.5% Triton-X 100 in PBS 1X. Subsequently, free-floating sections were incubated for 2 h with a blocking solution (0.5% Triton-X 100 and 2% horse serum in PBS 1X) at RT and incubated with primary antibodies in blocking solution for 72 h at 4 °C. Sections were then washed three times for 10 min in PBS 1X and subsequently incubated in 0.5% triton-X 100/PBS 1X at RT for 2 h with fluorophore coupled secondary antibodies. Sections were finally washed twice for 10 min in 0.1 M PB before mounting on glass slides using ProLong Gold Antifade reagent (Invitrogen). For analyzing the co-distribution of pTau and pSyn inclusions and for validating the 11A5 antibody staining, sections were incubated for an additional 20 min with the fluorescent DNA dye DRAQ7TM (1:100, Cell Signaling #7406) at RT and washed twice for 10 min in 0.1 M PB (pH 7.4) before mounting. See Tables 2 and 3 for references for primary and secondary antibodies. The immunostainings for Iba1, AT8, 4G8 or 11A5 antibodies that served for the analysis were done on consecutive slices. To improve homogeneity in the volumetric quantification analysis, samples were stained following the same combination of primary and secondary antibodies (respectively AT8 with anti-mouse Alexa Fluor 647, 4G8 with anti-mouse Alexa Fluor 488 and 11A5 with anti-mouse Alexa Fluor 488).

Image acquisition and analysis

2D image acquisition

All brightfield images of the FFPE DAB and hematoxylin-stained sections were captured by a light Leica brightfield

Table 2 Primary antibodies

Target	Epitope	Clone	Host species	Dilution	Manufacturer	Reference	RRID
pSyn	P-Ser129	11A5	Mouse (M)	1:500	Prothena Biosciences*	NA	NA
pSyn	P-Ser129	81A	Mouse (M)	1:200	Millipore	MABN826	AB_2904158
pSyn	P-Ser129	EP1536Y	Rabbit (M)	1:200	Abcam	ab51253	AB_869973
A β	AA17-24	4G8	Mouse (M)	1:200	BioLegend	800712	AB_2734548
Iba1/AIF-1	C-term	NA	Rabbit (P)	1:500	Wako	019-19741	AB_839504
NF-H	Met1-Ala380	NA	Goat (P)	1:500	Biotechne	AF3108	AB_2149640
pTau	Ser202, Thr205	AT8	Mouse (M)	1:500	ThermoFisher	MN1020	AB_223647
pTau	Ser422	NA	Rabbit (P)	1:150	ThermoFisher	44-764G	AB_1502115

M monoclonal, NA not available, P polyclonal

*Provided by Dr. Manuel Buttini

Table 3 Secondary antibodies

Fluorophore	Host	Reactivity	Isotype	Dilution	Manufacturer	Reference	RRID
Alexa Fluor 488	Donkey	Rabbit	IgG (H+L)	1:300	Jackson	711-545-152	AB_2313584
Alexa Fluor 488	Donkey	Mouse	IgG (H+L)	1:400	Jackson	715-545-150	AB_2340846
Alexa Fluor 488	Donkey	Goat	IgG (H+L)	1:400	Jackson	705-545-147	AB_2336933
Alexa Fluor 555	Donkey	Rabbit	IgG (H+L)	1:400	Invitrogen	#A-31572	AB_162543
Alexa Fluor 647	Donkey	Mouse	IgG (H+L)	1:300	Jackson	715-605-150	AB_2340862
Alexa Fluor 647	Donkey	Rabbit	IgG (H+L)	1:300	Jackson	711-605-152	AB_2492288

DM2000 LED microscope (Leica Microsystems) with 20× and 40× air objectives and a Leica DMC2900 camera (Leica Microsystems).

3D image acquisition

All confocal images for the MIC-MAC 2.0 analysis and for the quantification of pTau, A β and pSyn loads, 348 in total, were captured on a Zeiss LSM 710 with a 20× air objective. Some qualitative images were captured on a LSM 800 confocal system. 3D tile scans (z-steps of 1 μ m) of hippocampal subfields from age-matched CTLs, DLB and AD patients were stitched via Zeiss or Imaris Stitcher and visualized with Imaris 9.5 and 9.6 (Oxford Instrument). 3D stacks of Iba1 for microglia morphology and of pTau, A β and pSyn inclusions were acquired on serial sections in the anatomically defined regions of interest representative of the entire layered structure of the CA1, CA3 and DG/CA4: from *Stratum oriens* to *Stratum moleculare* for CA1 and CA3, and of the DG including the hilus (CA4) as indicated in Additional file 1: Fig. S1, online resource.

MIC-MAC 2.0

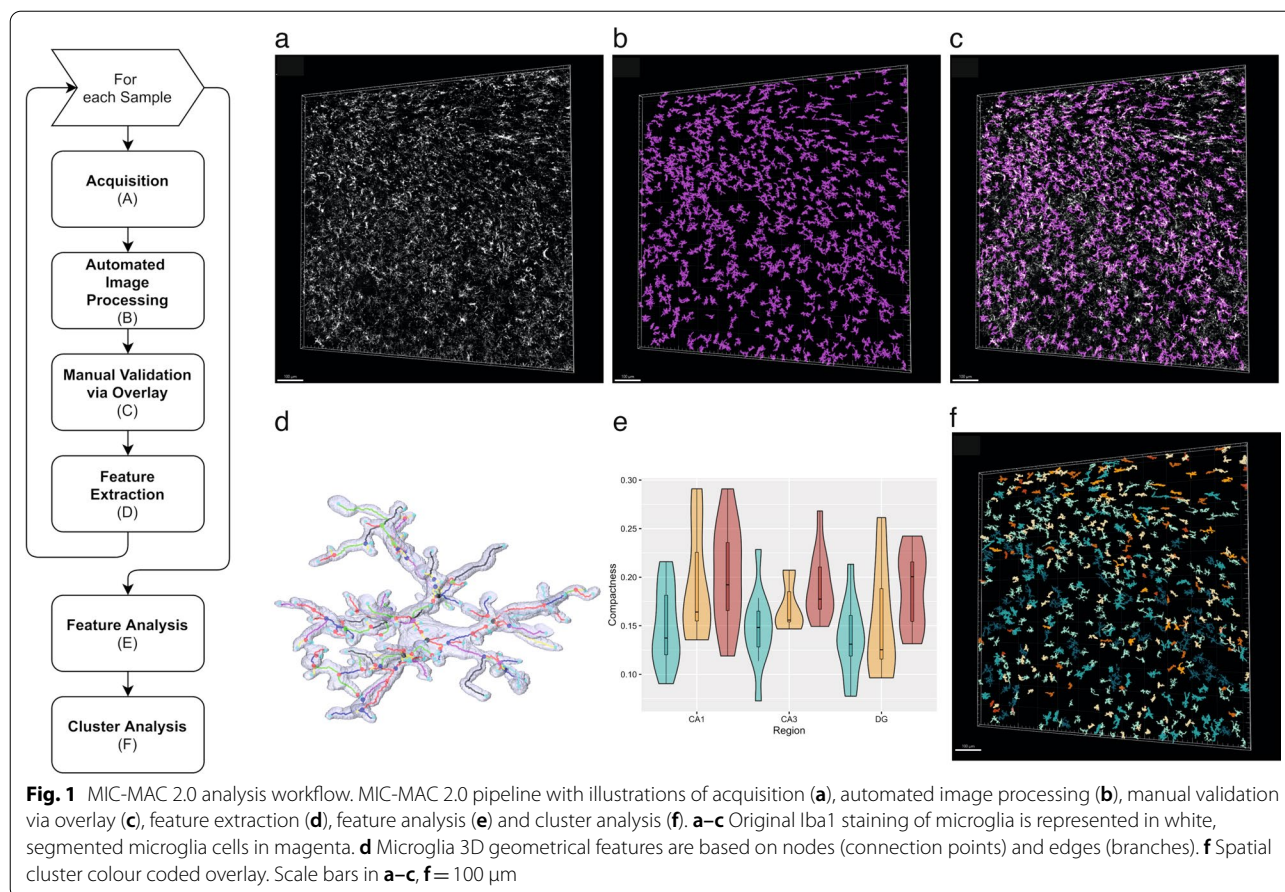
Microglia and Immune Cells Morphologies Analyser and Classifier (MIC-MAC) 2.0 is a pipeline that allows for automatic segmentation of microglia and immune cells from fluorescent microscopy 3D acquisition. With respect to the previous version [75], automation and time performance have been improved. Source code and training samples are available on: <https://doi.org/10.17881/w2d6-4934>.

New automated segmentation of microglia The image processing pipeline of MIC-MAC 2.0 is fully automated. While the previous version was based on a semi-supervised approach, meaning that a portion of the acquisition was needed to be labelled as positive signal or background, the new version automatically segments structures of interest by tuning parameters related to the image processing pipeline. A flowchart of the image processing pipeline is presented in Fig. 1. The algorithm works by elaborating the 2D images of the 3D stacks one by one. First, a

noise filtering is applied [22] with $\sigma=25$, followed by a background subtraction phase made with a Gaussian filter ($\sigma=[10-50]$). After an intensity adjustment [matlab::imadjust], the image is deconvolved by using the Lucy-Richardson method [50, 71]. Finally, positive pixels are detected via global thresholding by defining a parameter for the threshold t . The only two parameters that have been changed throughout this phase are σ from the Gaussian filter and t from the global thresholding. The parameters have been tuned accordingly to the amount of noise present in the image, which can change due to numerous factors (e.g., microscope parameterization, tissue conservation and antibody penetration). All morphologies of microglia were further validated by overlaying the segmented microglia object on the original 3D stack with the Iba1 staining.

Feature extraction and selection Automated morphological feature extraction is performed at individual cell resolution [75]. Out of 62 morphological features and derived measures from the first version of MIC-MAC, we have selected a subset of 16 features by discarding highly correlated features (Pearson, higher than 80%). Among the 16 features are morphological and graph-based measures representing distinct aspects of the 3D morphology to measure fine changes and alterations. A detailed description of the 16 features can be found in Additional file 1: Fig. S3, online resource, with an illustration of prototypical minimum and maximum extreme values.

Artifact removal Segmentation artifacts were automatically removed in three different steps: (1) By thresholding cell volume and keeping cells whose volume is between $\sim 48,000$ and $\sim 216,000$ μm^3 . The volumetric range was visually validated. (2) By considering the amount of cell body surface that is included in the border of the acquisition. This allows to exclude cells whose shape is incomplete and thus may alter the results. We specifically remove cells whose shared surface with the border is bigger than 7.5% of the total cell surface. This threshold has been manually tuned by visual validation. (3) By training



a classifier based on morphological features. We trained a classifier (Boosted Tree–Ada Boost) [29] via manual labelling of artifacts and applied the classification to the whole dataset with k-fold validation to prevent overfitting. The removal via cell volume is performed right after the image processing segmentation in order to speed up the feature extraction phase. The latter two, are performed after the feature extraction phase right before the analysis. Feature and cluster analyses are performed on a total of 32,447 individual microglia morphologies.

Cluster analysis All 16 selected features were initially normalized to the range 0 to 1 over the complete set of cells. We used Ward hierarchical clustering [93] on the set of 16 features. All the features have been normalized by range into a mapping from 0 to 1 renderings of cells belonging to specific clusters at different heights of the dendrogram. We assessed that $n=7$ was the best set-up to segregate distinct morphological clusters. These differences were further validated by the statistical analysis of features distribution among clusters (Additional file 1: Fig. S4, online resource). Cells were subsequently pro-

jected on a Uniform Manifold Approximation and Projection (UMAP) [58] for visualization purpose.

Volumetric quantification of pTau, A β and pSyn pathologies

3D stacks were acquired following the same parameters for confocal laser scanning (magnification, resolution, laser power, offset and dwell time). All subfields were acquired from the same slide. All segmentations of the protein inclusions were done on Imaris 9.5.1 and 9.6 with the surface module following the same procedure for each marker (surface detail, absolute intensity, thresholds). After segmentation, all volumes of the resulting objects (3D reconstructions) were summed up. The final score (%) represents the percentage of the volume of the stack covered by the selected marker staining.

Statistical tests

For statistical comparisons between populations, we used Mann–Whitney U Test. For evaluating score and p-value of correlations we used Spearman Correlation. All tests were performed at a significance level of 5%. In accordance with the explorative nature of the analysis, no correction for multiple testing was necessary.

Results

Microglia morphological responses in hippocampal subfields of AD and DLB patients

To assess the subregional microglia responses that paralleled the local pathological context, we took advantage of the Microglia and Immune Cells Morphologies Analyser and Classifier (MIC-MAC) pipeline [75] that allows for semi-automated segmentation and classification of microglia cells based on their morphologies. Indeed, morphologies of microglia partially reflect their responses; surveying microglia are usually very ramified, whereas activated microglia present an amoeboid-like morphology. To improve time-consuming imaging and analytical processing, we implemented numerous changes to create a MIC-MAC 2.0 version which is now available for research as open source (<https://doi.org/10.17881/w2d6-4934>). MIC-MAC 2.0 allows a fully automated, more precise and faster segmentation of large 3D confocal stacks, an automated discard of the stack-border microglia that could create artifact structures (Fig. 1). For this study, we captured more than 43,000 Iba1-positive objects across 87 3D stacks, representative of each of the three hippocampal subfields for each case of our cohort. Before analysis, we found slight variations but no statistical differences on Iba1 staining density across subfields and conditions (Additional file 1: Fig. S2, online resource). After segmentation, MIC-MAC 2.0 imposed a volume threshold to select individual microglia but discard microglia accumulations that appeared as merged structures, such as the A β plaque associated microglia. In our hands, individual cellular boundaries of microglia forming accumulations around the plaques cannot be delimited even after stimulated emission depletion (STED) microscopy super-resolution imaging (data not shown), which justified their exclusion from our analysis. After the removal of artifactual objects, we obtained 32,447 individual cell 3D reconstructions validated for our analysis. MIC-MAC 2.0 retained 16 of the previous 62 morphological and graph-based features from MIC-MAC that were shown to recapitulate the complexity of microglia morphologies based on arborization and core parameters of 3D morphology such as volume or polarity (Additional file 1: Fig. S3, online resource).

Variations of microglia morphological features across hippocampal subfields in AD and DLB cases

First, we measured the 16 morphological features of extracted microglia (list, definition and examples of their maximum and minimum prototypical structures in Additional file 1: Fig. S3, online resource) to assess the precise changes in their morphologies across subfields and conditions (Fig. 2). Interestingly, DLB values presented a

similar trend to AD samples for almost all features and subfields when compared to CTLs, but without reaching significance. Among the 16 features, we found only four of them significantly different in AD compared to CTLs in at least one subfield. The compactness was the only feature significantly increased in all subfields in AD compared to CTLs ($P < 0.05$ for CA1 and CA3, $P < 0.001$ for DG/CA4) (Fig. 2a). High values for compactness are corresponding to amoeboid morphologies. Volume/number of edges significantly increased, and node density decreased in CA1 (both $P < 0.05$) and DG AD (respectively $P < 0.05$ and $P < 0.01$) (Fig. 2b, c). High values for volume/number of edges and low values for node density are matched with a simplified morphology with few or no branches. Ending nodes density increased in CA3 AD ($P < 0.05$) and indicates the enrichment of microglia with a low number of principal branches without secondary branches (Fig. 2d). Intra-condition, we found that the feature average node degree is significantly higher in CA1 AD than in CA3 and DG/CA4 AD ($P < 0.05$ and $P < 0.05$; Fig. 2e), s-metric and node density lower in CA3 than DG/CA4 in DLB ($P < 0.05$ Fig. 3f, and $P < 0.05$ Fig. 2c). Overall, compared to the CTLs microglia from the same subfield, CA1 AD microglia population adopted a morphology with higher compactness and loss of branching. AD DG/CA4 microglia followed a similar trend but to a lesser degree. AD CA3 microglia also showed a decrease in their complexity but with a distinct fine-tuning of their morphology.

Microglia morphological clusters composition in the hippocampus AD and DLB patients

Feature analysis allowed us to dissect the fine details of microglia morphologies. To further characterize how microglia populations are remodeled across the hippocampal subfields in AD and DLB, we applied a cluster analysis to our matrix of morphological data. Briefly, we have selected seven clusters after a Ward hierarchical clustering based on a normalized set of the 16 features (Fig. 3a). The seven clusters showed distinct morphological patterns with specific characteristics and were distributed accordingly on an UMAP (Fig. 3b, c, Additional file 1: Fig. S4a–c, online resource). Briefly, clusters 1, 2 and 7 were composed by branched and complex cells but showed clear differences in their volume and polarity (high for cluster 1, intermediate for cluster 2 and low for cluster 7). Cluster 3 represented the most compact and smallest microglia. Clusters 4, 5 and 6 showed intermediate shapes mainly segregated by distinct features such as volume (higher in cluster 5), mean edge length (higher in cluster 4), and node density (higher in cluster 6) (Additional file 1: Fig. S4d–i, online resource). We then analyzed clusters relative abundances across conditions

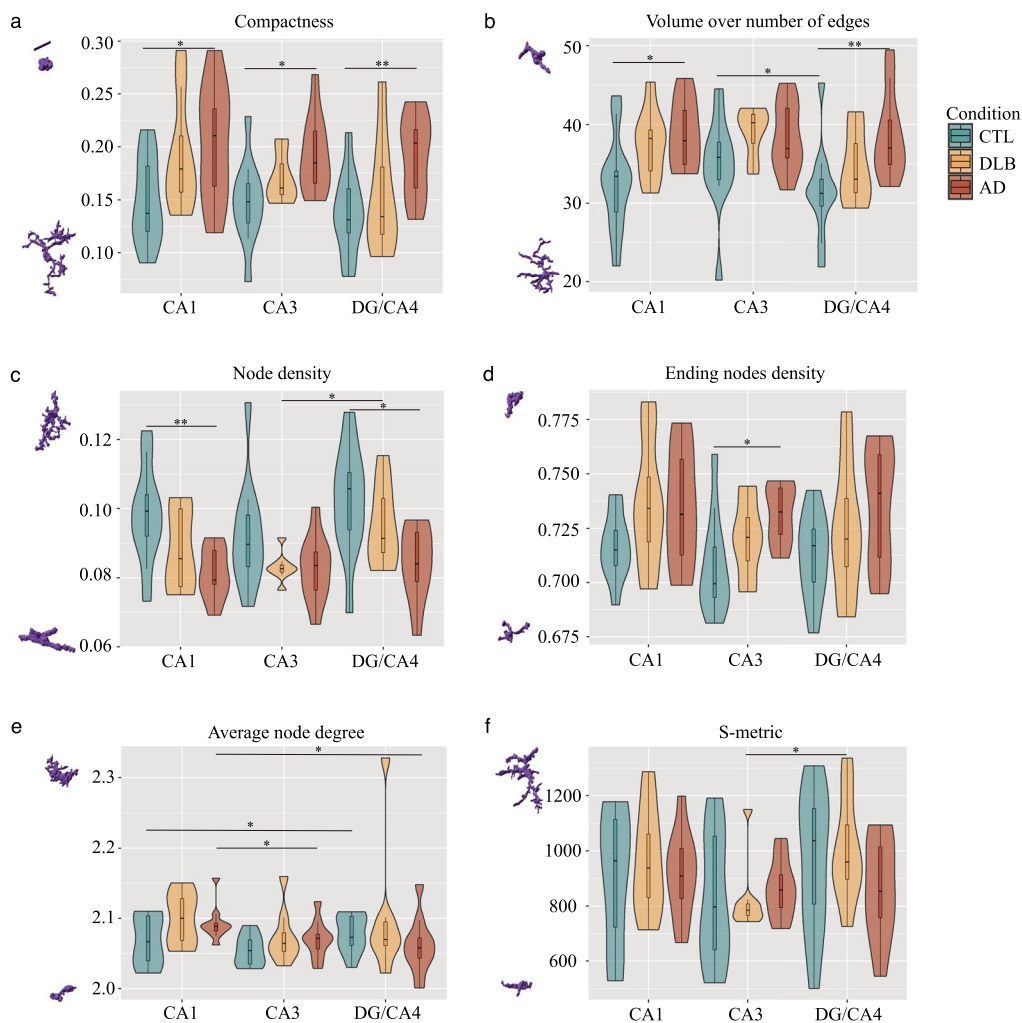


Fig. 2 Subregional morphological alterations of microglia in the hippocampus of AD patients. Using MIC-MAC 2.0, we have extracted 16 geometrical features per cell of 32,447 individual microglia collected in CA1, CA3 and DG/CA4 subfields from AD, DLB and age-matched CTLs. None of the analyzed microglia morphological features was significantly changed in the DLB samples but follow a trend similar to the AD condition. All the following reported changes are observed in AD vs CTL samples. **a** Compactness is significantly increased in all three hippocampal subregions, **b** and volume over number of edges is significantly increased in CA1 and DG/CA4. **c** Node density significantly decreases in CA1 and DG/CA4, as does ending nodes density in CA3 **(d)**. Two features, namely average node degree and s-metric present significant intra-condition regional changes **(e, f)**. Wilcoxon–Mann–Whitney U-test *P* values are indicated in the graphs: **P* < 0.05 and ***P* < 0.01. Scaled prototypic morphologies with highest and lowest value for the selected feature have been added on the left side. Scale bar = 20 μm

(See figure on next page.)

Fig. 3 Microglia morphological cluster distribution varies according to the disease and the hippocampal subfield. Ward hierarchical clustering on the matrix of 32,447 microglia based on 16 features defines seven distinct morphological clusters. **a** Hierarchical clustering dendrogram. **b** Projection on a UMAP of the seven clusters where each of 32,447 individual microglia is represented by a dot. **c** Scaled prototypical morphologies of microglia associated to the seven clusters inside the UMAP. **d, e** Histograms showing the variation in abundance (average composition in %) of the seven clusters according to the condition **(d)** and across subfield per condition **(e)**. Overall, clusters 3 and 5 are enriched in the disease conditions, whereas cluster 7 is depleted. Scale bar in **c** = 30 μm. Wilcoxon–Mann–Whitney U-test *P* values are indicated in the graphs: **P* < 0.05; ***P* < 0.01 and ****P* < 0.001

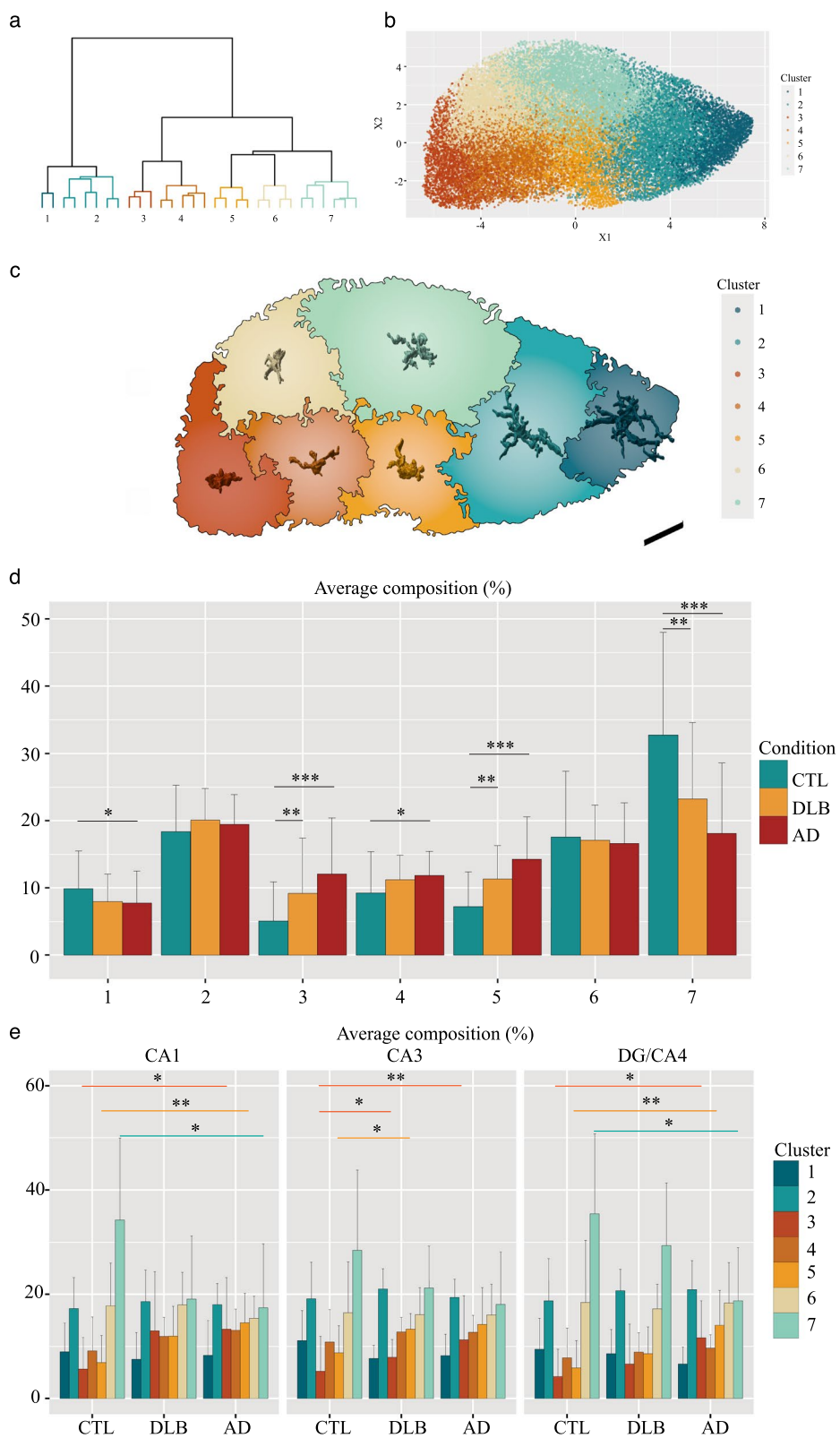


Fig. 3 (See legend on previous page.)

(Fig. 3d). We found a general decrease of two of the most ramified clusters, 1 and more severely of 7, in AD compared to CTLs (respectively $P < 0.05$ and $P < 0.001$) and of 7 in DLB ($P < 0.05$). Cluster 3 and 5 were enriched in both disease conditions compared to CTLs (cluster 3: AD $P < 0.001$, DLB $P < 0.01$) (cluster 5: AD $P < 0.001$, DLB $P < 0.01$). Clusters 2 and 6 stayed stable across conditions and cluster 4 was slightly but significantly increased in AD vs CTLs ($P < 0.05$). We then analyzed the changes of cluster composition by subfield across conditions (Fig. 3e). We reached significance for cluster 3 increase for all subfields in AD compared to CTLs ($P < 0.05$ in CA1; $P < 0.01$ in CA3 and $P < 0.05$ in DG/CA4) and in CA3 DLB ($P < 0.05$); for cluster 5 increase in CA1 AD, DG/CA4 AD ($P < 0.01$) and CA3 DLB ($P < 0.05$), and for cluster 7 decrease in CA1 and DG/CA4 AD ($P < 0.05$). These results show that microglia follow the same trends in AD and DLB cases compared to age-matched CTLs. However, they are less pronounced in DLB. At the sub-regional level, strong remodelling affects the CA1 and DG/CA4 microglia populations in AD and the ones of

the CA3 in DLB. Additionally, the morphological cluster composition might highlight a microglia functional heterogeneity. Some clusters specifically changed depending on the subfield and condition. In particular clusters 3 and 5, two morphologically distinct groups, were enriched in disease conditions. Other clusters such as 2 and 6 appeared unaffected by the pathological context.

Co-occurrence and severity patterns of pTau, Aβ and pSyn pathologies in the hippocampal subfields of AD and DLB samples

To assess how microglia changes were affected by the subregional pathological context, we then employed confocal microscopy to measure pTau, Aβ and pSyn loads across subfields and conditions in consecutive sections. The analysis of the fluorescent staining of AT8 for pTau and 4G8 for Aβ antibodies, which are typically used for neuropathology assessment, showed expected inclusions and labeled structures, i.e., typical paired helical filaments (PHF) and NFTs with AT8 [32], Aβ plaques and some amyloid precursor protein (APP) detected

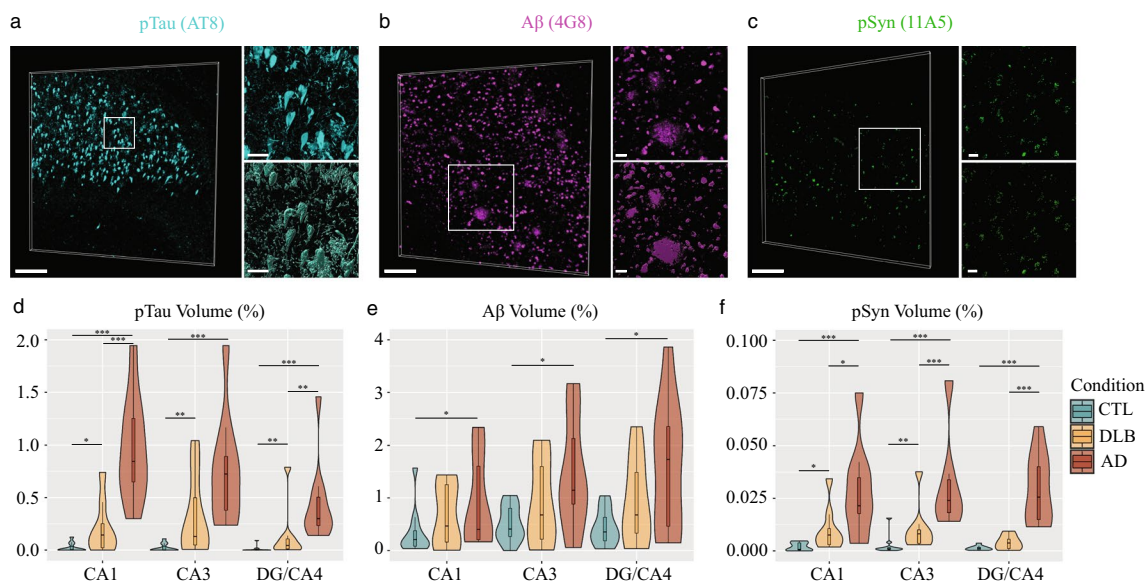


Fig. 4 PTau, Aβ and pSyn loads show distinct disease-associated, subregional patterns in the hippocampus of AD and DLB patients. PTau, Aβ, and pSyn burdens were assessed via immunofluorescence staining (big panels and zoom in small upper panels) and volumetric analysis in CA1, CA3 and DG/CA4 of age-matched CTLs, AD and DLB patients. The staining signal was segmented (with Imaris 9.6) (small lower panels) and their volume measured from 3D acquisitions of each hippocampal subfield for each sample. **a** PHFs and NFTs of pTau (cyan) were stained with anti-AT8, example of an 80-year-old male AD patient (case 21). **b** Aβ plaques and subcellular inclusions (magenta) were stained with anti-4G8, example of a 90-year-old male AD patient (case 30). **c** pSyn inclusions, Lewy bodies and Lewy neurites (green) were stained with anti-11A5, example of a 64-year-old male DLB patient (case 15). Violin plots (with box plots) show that **d** PTau levels are significantly higher in the AD samples as compared to both DLB and CTLs in all three hippocampal subfields, but a significant increase was also observed in DLB samples compared to CTLs. **e** Aβ levels are significantly higher in AD samples in all three subfields compared to CTLs, whereas no significant differences are seen between DLB and both AD and CTLs. Aβ loads follow the same subregional pattern in DLB but with lower values. **f** pSyn loads are significantly increased in AD in all subfields, and in CA1 and CA3 in DLB compared to age-matched controls. pSyn volumes in all subfields are also significantly higher in AD samples compared to DLB. Wilcoxon–Mann–Whitney U-test P values are indicated in the graphs: * $P < 0.05$; ** $P < 0.01$ and *** $P < 0.001$. Scale bars in **a–c** big panels = 200 μm, small panels = 30 μm

in neuronal soma with 4G8 [37] (Fig. 4a, b; Additional file 1: Fig. S5, online resource; Additional file 1: Fig. S6, online resource). The 11A5 pSyn staining revealed multiple types of inclusions, from Lewy neurite-like structures to intracellular granular staining (Fig. 4c; Additional file 1: Fig. S6, online resource). To validate the 11A5 antibody against PS129 pSyn, we immunostained 3 μ m thick FFPE sections of the amygdala from a DLB case with 11A5, 81A (Millipore) and EP1536Y (Abcam) antibodies all directed against the same PS129 target. All antibodies revealed a similar pattern typical of pSyn pathology such as Lewy neurites, Lewy bodies and intracellular vacuolar aggregations in neurons (Additional file 1: Fig. S7a, online resource). We then immunostained thick sections of formalin-fixed subiculum-entorhinal cortex of the same case, with a combination of an anti-PS129 antibodies (11A5, 81A or EP1536Y), an antibody against pan-axonal neurofilament to detect neurons (NF-H) and DRAQ7TM to stain nuclei and analyzed the 3D confocal images (Additional file 1: Fig. S7b, online resource). Again, all PS129 antibodies gave a broadly similar staining with labeled structures resembling Lewy bodies and Lewy neurites found enclosed in neurons double-stained for NF-H and DRAQ7TM. The 11A5-positive structures found in our cohort of AD and DLB samples resembled Lewy neurites and Lewy bodies but also revealed cellular inclusions and PHF-like structures, which were also seen with the 81A antibody (Additional file 1: Fig. S8, online resource).

After validation of the 11A5 antibody, we acquired representative 3D image stacks of AT8, 4G8 and 11A5 staining of the CA1, CA3 and DG/CA4 subfields for each case. The images were segmented to estimate the relative volume covered by the pathology of interest (Fig. 4a–c). We found variations in the pathological protein loads across samples and conditions that were generally compatible with the neuropathology staging of the samples. However, we observed all three pTau, A β , and pSyn pathologies in AD as well as in DLB cases. The majority of DLB cases were already described with partial AD pathologies and we found low to intermediate levels of pTau, A β , and pSyn accumulations (Fig. 4d–f). The AD group showed the highest levels for all pathologies, including pSyn, in the three hippocampal subfields. The CTLs showed no or low level of pTau staining and low to moderate A β labelling in neuronal-like soma and in few extra-cellular deposits. In our CTL group, we also observed very few pSyn inclusions in cells looking like pyramidal neurons but no Lewy bodies or Lewy neurite like structures.

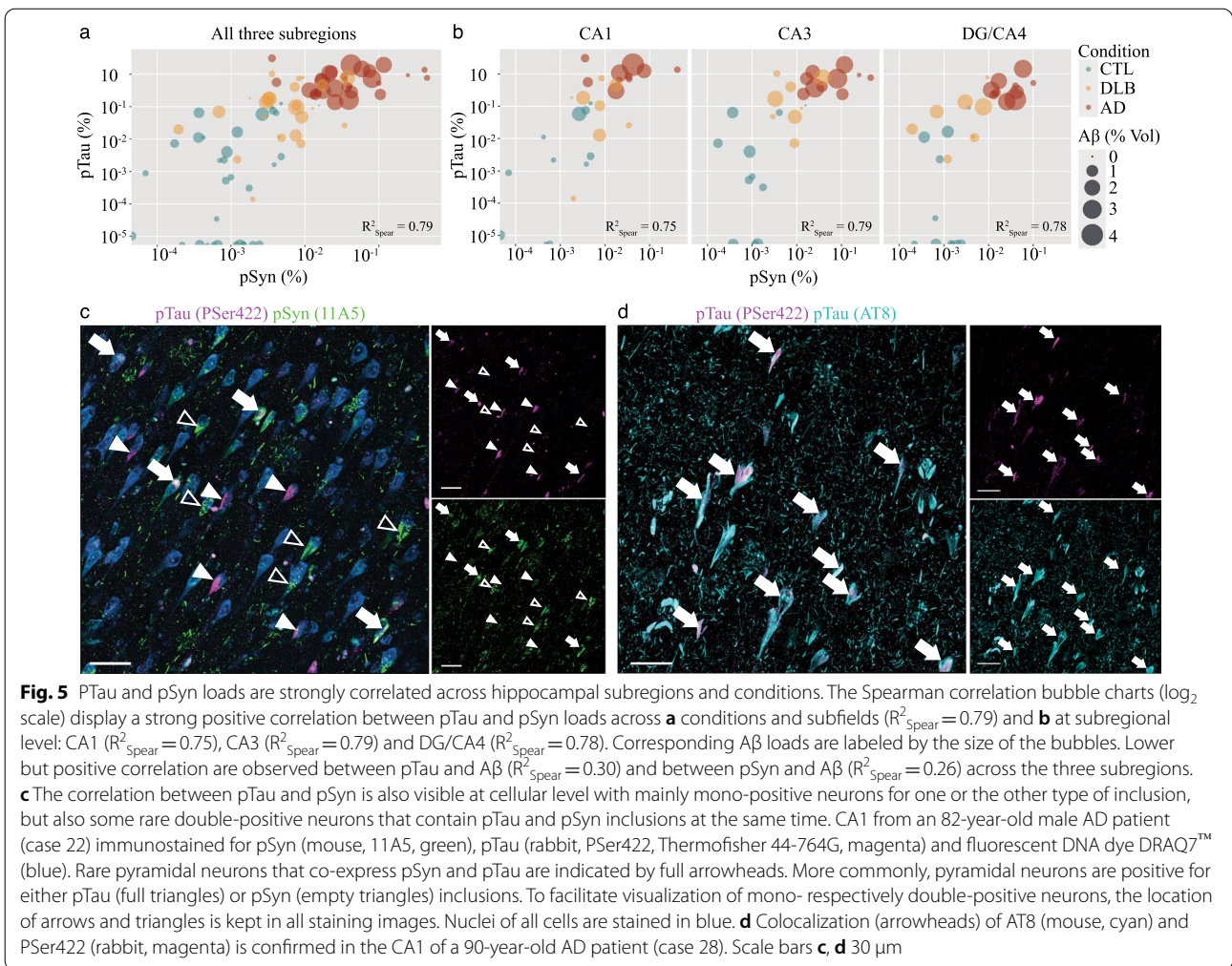
More precisely, pTau burdens were significantly higher in all subfields in AD and DLB compared to CTLs (AD vs CTLs: $P < 0.001$, DLB vs CTLs: $P < 0.05$) and followed a similar subregional pattern across conditions with the

highest loads found in CA1 and CA3 and lowest in DG/CA4. The severity of the pTau pathology was considerably higher with the most extreme values in CA1 AD, and DG/CA4 AD compared to DLB respective subfields ($P < 0.001$ in CA1; $P < 0.05$ in DG/CA4). We found a distinct subregional pattern of A β loads, again, conserved across the conditions with the highest A β burdens in DG/CA4 and CA3 and lowest in CA1. Only A β AD values were significantly higher than CTLs ones for all subfields ($P < 0.05$). The subregional distribution of pSyn loads appeared more uniform across subfields but with the highest loads found in CA1 and CA3 in AD and DLB. Still, the volume recovered by pSyn staining were very low compared to A β or pTau ones. We found statistical significances for all subfields compared to CTLs for AD ($P < 0.001$), and for CA1 ($P < 0.05$) and CA3 ($P < 0.01$) in DLB. Surprisingly, the pSyn burdens were much higher in AD than DLB samples for all subfields ($P < 0.05$ CA1, $P < 0.001$ CA3 and DG/CA4). Our data suggest that pTau, A β and pSyn pathologies follow a specific subregional hippocampal pattern that is shared across AD and DLB. However, burdens were more severe in AD, with CA1 AD particularly affected by pTau accumulations.

Next, we examined the association between the three pathologies across subfields and conditions (Fig. 5a, b). Positive associations between pTau and A β and between pSyn and A β volumes of respectively $R^2_{\text{Spear}} = 0.30$ and 0.26 were found across subfields and conditions but differ subregionally with superior values in the CA1 (respectively $R^2_{\text{Spear}} = 0.42$ and 0.37 ($P < 0.05$)) and a loss of statistical significance in the CA3 and DG/CA4. However, we found a strong positive correlation between pTau and pSyn volumes across conditions ($R^2_{\text{Spear}} = 0.79$; $P < 0.001$) that was preserved in all subfields (CA1: $R^2_{\text{Spear}} = 0.75$; CA3: $R^2_{\text{Spear}} = 0.79$; DG/CA4: $R^2_{\text{Spear}} = 0.78$; $P < 0.001$). To better define pTau and pSyn associations at the cellular level, we tested double staining of pTau with a Pser422 rabbit antibody to pair with the 11A5 mouse antibody and DRAQ7TM (Fig. 5c). We also confirmed that stainings with pTau Pser422 (rabbit) and AT8 (mouse) colocalized in a CA1 AD case (Fig. 5d). We observed a global co-distribution of pTau and pSyn in the same microenvironment, however, colocalizations in the same neuron were sparse and mono-stained neurons more common. Thus, the strong positive correlation between pTau and pSyn does not point out intertwined intracellular co-pathologies but rather simultaneous mono pTau or pSyn accumulations in neighbouring hippocampal neurons.

Associations between morphological microglia changes and pTau, A β and pSyn loads in AD and DLB hippocampi

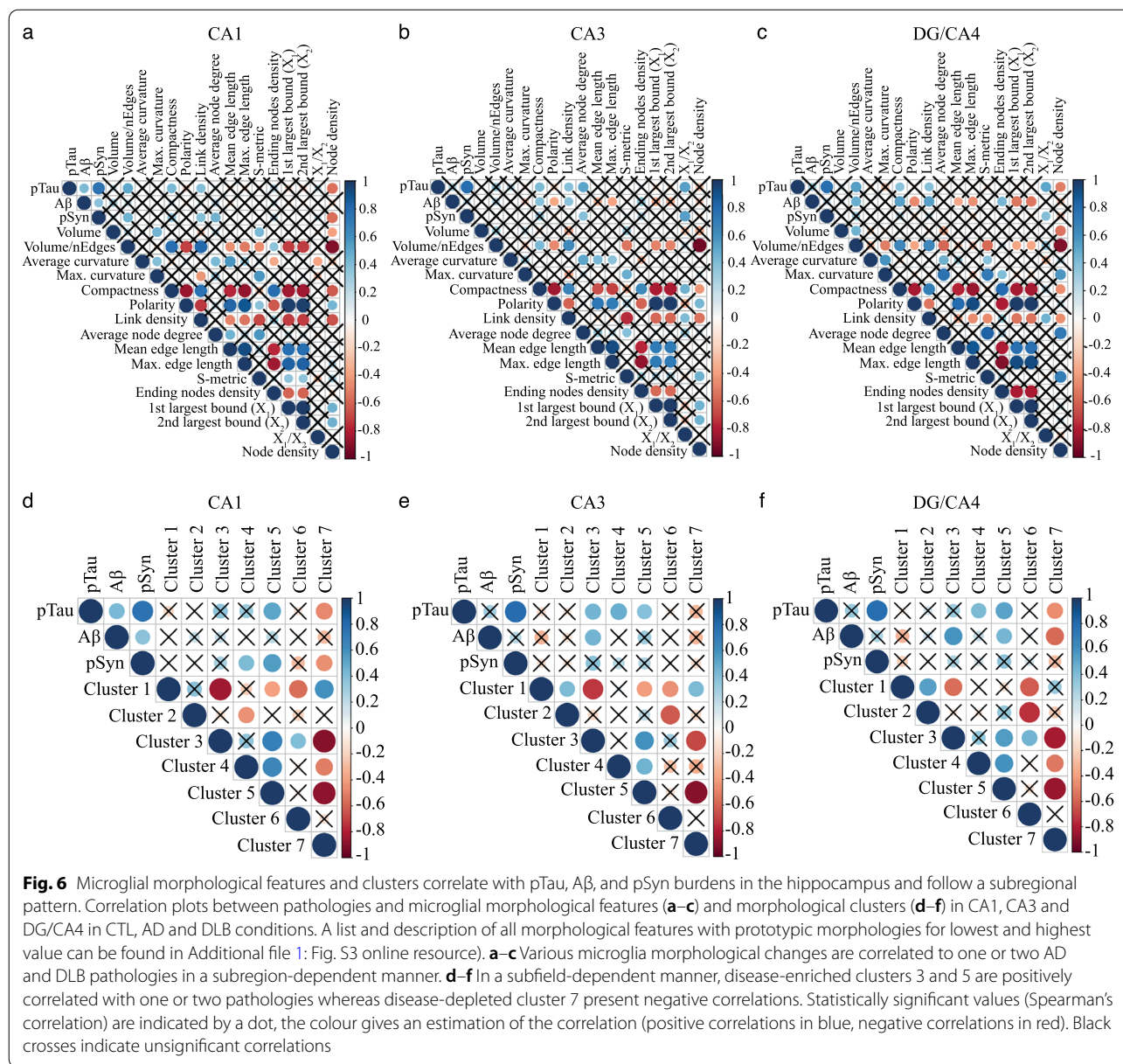
To evaluate the relationship between microglia responses and each pathology at the subregional level across



conditions, we first evaluated the correlations (Spearman, statistically significant) between morphological features and pTau, A β or pSyn burdens across subfields (Fig. 6a–c). We found that the associations of pTau, A β and pSyn with features changed across subfields. In the CA1, pTau loads were correlated with some of the most altered features in DLB and AD, volume/number of edges, compactness, node density, and link density, a feature related to the complexity of the arborization. PSyn loads showed similar values of correlation than pTau ones with numerous features such as volume/number of edges, node density, and link density, but did not correlate with compactness and were positively associated with average node degree. Thus, we found a trend of correlations between the most altered features and a tandem of pTau and pSyn pathologies in the CA1 but an absence of statistically significant correlations with A β . In the CA3, some features were significantly associated with pTau (4) in tandem with A β (2) or pSyn (2), and 3 features uniquely to A β . In DG/CA4, a higher range of

features were positively or negatively associated with A β (8), sometimes in tandem with pTau (3), with pTau alone (1) and pTau together with pSyn (1). The compactness, a feature statistically increased in AD, was associated with pTau loads in all subfields, but in tandem with A β only in the CA3 and DG/CA4. Volume/number of edges also changed in AD CA1 and DG/CA4, and showed an association with both pTau and pSyn in the CA1, and with pTau and A β in DG/CA4. Some features were specifically associated with one pathology such as node density with pTau or polarity, max and mean edge length, ending node and 1st and 2nd largest bound with A β . Overall, pTau in tandem with pSyn pathology seems to drive the most significant changes in the CA1 microglia, however A β , when highly expressed such as in DG/CA4, remains a potential dynamic modifier of microglia morphology.

At the cluster level, we also found a strong effect of the subregion on the associations between pathologies and clusters (Fig. 6d–f). In the CA1, we found positive correlations between cluster 5, the most branched of the



disease-enriched cluster, and negative ones for cluster 7 composed by highly ramified cells, and the duo of pTau and pSyn loads, and a positive correlation between cluster 4 and pSyn. In the CA3, cluster 3 was positively correlated with the pair of pTau and Aβ loads, clusters 4 and 5 with pTau loads. In the DG/CA4, cluster 3 was associated with Aβ loads only and cluster 4 with pTau ones only, cluster 5 and 7 with the pair of pTau and Aβ loads.

This correlative analysis implies that each pathology impacts a specific set of morphological features of microglia but can also work in synergy with others to transform microglia toward clusters 3 and 5 morphology types. At the cluster level, the impact of pSyn is lower. pTau seems

to be the stronger modifier in the CA1 and CA3 subregions, Aβ in the DG/CA4. Across subfield, pTau maintains a strong positive association with cluster 5 while cluster 3 is more correlated to Aβ. These data suggest that the severity, distribution but also co-occurrence of the three pathologies impact microglia phenotypic heterogeneity and condition their responses.

Discussion

Our study offers a transversal and high-resolution description of the local morphological phenotypes of microglia in the hippocampal CA1, CA3 and DG/CA4 subfields across age-matched CTLs, AD and DLB

conditions and their association with the subregional distribution and severity of the pTau, A β and pSyn pathologies. We have obtained high-content data about subregional patterning of pathologies in the human hippocampus in DLB and AD cases and unveiled its relationship with the remodelling of the microglia local population.

Hippocampal microglia morphological remodelling is subregional and more severe in AD compared to DLB cases

Morphology of microglia only partially reflect their responses. However, visual description is commonly used to obtain a rapid readout of their alterations in CNS diseases. Indeed, the homeostatic microglia harbour a highly ramified profile in contrast to activated microglia that appear smaller, amoeboid-like with no or low number of branches. Here, we have analyzed 3D morphologies to characterize the local reorganization of microglia populations in hippocampal subregions of AD and DLB patients. We previously developed an AI pipeline called MIC-MAC, to classify and quantify morphologies of individual microglia labelled with the Iba1 marker in large 3D confocal image stacks of human or mouse post-mortem brains [75]. With MIC-MAC 2.0, we have significantly improved the automation and precision of the segmentation and added new features to discard artefacts upstream from the analysis. A caveat of our approach is that MIC-MAC 2.0 automatically discards all microglia accumulations, where the cells are so closely intermingled that our pipeline cannot separate them into individual cells after the segmentation process. In our hands, even super-resolution microscopy could not resolve the human microglia cellular boundaries in these accumulations. This argument strengthened our decision to focus on individual cells to overcome potential contaminations in our data but created a limitation and lowered the impact of A β on microglia changes in our analysis. However, we have created a substantial amount of information based on a sampling of 32,447 extracted individual microglia. By quantifying their 16 morphological features, our analysis highlighted disease and subregional particularities. When compared to their respective subfield in CTLs, we found statistical significances only for the AD condition. However, DLB variation trends always mimic AD ones showing that the presence of concomitant pathologies already initiated local remodelling but in a more subtle manner. Other reports found low to mild microglial changes in DLB samples with different approaches. Their conclusions were supported by 2D morphology analyses and quantifications of some activation markers in the hippocampus [6] and other brain areas such temporal lobe, the superior frontal gyrus

[86] and the cerebral cortex [2]. However, our analysis implies that DLB hippocampal microglia are not so different from AD ones in their ability to respond and that their alterations are associated with the local level of severity of DLB- and AD-typical pathologies. High compactness was the only predictive feature for AD across subfields, strengthening the observation that microglia tend to become more amoeboid in AD, even when not attached to the plaques. At the morphological clusters level, in line with previous studies [6, 66], we show a decrease of the most branched and tortuous subgroups and an increase of amoeboid-like clusters significantly in AD. Interestingly, the low levels of the disease-increased clusters found in CTLs could be products of the ageing process or the onset of pathological mechanisms [14]. Our data also further suggest functional heterogeneity among microglia local subgroups. Indeed, we found that two morphological clusters stayed relatively stable over the conditions, while others were specifically depleted toward simplified morphologies. We have also uncovered two stereotypical morphologies enriched in AD and DLB, one amoeboid-like and one semi-ramified, which could reflect differential responses to pathological stressors [56]. PET imaging studies associated microglia activation with volume loss [25]. Here the increase of clusters 3 and 5 in AD and to a lower level in DLB samples is in line with this report and the more severe atrophy of the hippocampus observed in AD cases [1, 3, 40, 43, 53, 74, 96]. We also found a subregional remodelling of microglia populations that highlights more profound alterations in CA1 AD. Our quantitative analysis of pTau, A β and pSyn loads unveiled a tight and synergistic effect of the local misfolded protein pathologies with microglia changes.

pTau, A β and pSyn burdens overlap and show specific subregional patterns in the hippocampus of AD and DLB cases

Here we report a high co-occurrence of the three types of pathologies studied, pTau, A β , and pSyn in the hippocampal subfields of AD and DLB cases. We have observed some low A β staining and pSyn accumulations but almost no pTau inclusions in our age-matched non-demented CTLs, in line with previous reports [21, 39, 42, 45, 54, 73]. With our 3D confocal approach, we found that pTau, A β and even pSyn burdens were all more severe in AD. The concomitance of pTau, A β , and pSyn loads is commonly observed in age-related neurodegenerative diseases [33] in both AD and DLB [60, 72] in numerous brain areas [17, 27, 81, 92]. However, our study revealed a complex tapestry of subregional pathological imprint in AD and DLB hippocampi, which each of the pathologies showing a specific subfield pattern. We found that pTau loads were more enriched

toward CA1 and A β ones toward DG/CA4. pSyn loads were slightly higher in CA1 and CA3 but appeared more homogeneous across subfields. DLB samples presented intermediate values of pTau, A β and pSyn pathologies. Overall, our data are consistent with existing literature regarding the subregional distribution of pTau pathology in AD and DLB [11, 19], but slightly differ regarding A β subregional distribution [88] and pSyn higher loads in AD. The pSyn burden observed in the hippocampus across AD and DLB cases was very mild compared to A β and pTau ones. However, confocal microscopy allowed us to reveal frequent pSyn intracellular granular inclusions in cells identified as pyramidal neurons along with typical Lewy neurites and few Lewy bodies that might uncover an early sequence of pSyn pathology. Interestingly, we report stronger associations between pTau and pSyn burdens than between pTau or pSyn and A β loads. We found that the strong positive correlation between pTau and pSyn pathologies depended mainly on an exclusive distribution of pTau or pSyn inclusions in neighbouring hippocampal neurons rather than on a colocalization in the same cell, an observation that could suggest a systematic mechanistic association. However, we observed few double-positive hippocampal neurons carrying pTau and pSyn pathologies such as previously found in the subiculum [38], the amygdala [80] and parahippocampal gyri [35] in AD and DLB cases. In a previous study, the local co-distribution of NFTs and Lewy bodies was found more frequent in limbic areas than other brain parts [17]. Tau and synuclein proteins seem to be part of the same interactome in induced pluripotent stem cells (iPSC)-derived neuron models [89] but our observations contradict the idea of a stereotypic dual pathology in the AD and DLB hippocampus. How pSyn- and pTau-bearing neighbouring neurons co-inhabit the AD and DLB hippocampus and how the two pathologies coincide in few others remains to be understood. AD and DLB are complex diseases, and our study faces some limitations for generalizing our neuropathology findings such as the number of cases (29) included in our analysis. However, we did not evaluate the impact of TAR DNA binding protein of 43 kDa (TDP-43) pathology. Abnormal accumulations of TDP-43 in neurons were originally associated with frontotemporal lobar degeneration and amyotrophic lateral sclerosis. TDP-43 inclusions are now frequently reported in AD [62] and DLB+AD cases [65] and could play a substantial role in the hippocampal atrophy rate [41]. Finally, we have analyzed the medium part of the hippocampus, i.e., the body, between the uncus and *Corpus geniculatum laterale*, a region which is usually poorly described, contrary to the head at the uncus level or the tail close to the

Corpus geniculatum laterale, both more regularly used for neuropathology diagnostic and research. We cannot exclude differences with previous reports as it has been shown that the hippocampus is molecularly and functionally diverse along its longitudinal axis [5, 85] and may be affected by different local levels of pathologies.

Combinatory pattern of pTau, A β and pSyn loads and coinciding microglia responses shape the subregional deterioration of the hippocampus

Our study demonstrates that the combinatory pattern and the severity of pTau, A β and pSyn pathologies are associated with specific local microglia responses within the hippocampus. Each of pTau, A β and pSyn pathology seems to impact, often in tandem, the local microglia remodelling in AD and DLB hippocampi. We found fine-tuned associations with specific features or clusters that reflect the tight interdependence of microglia states with their microenvironment. Indeed, the correlation analysis showed that pTau and A β pathologies can be positively or negatively associated with a specific set of morphological features even if they also seem to work in synergy on some others. pSyn pathology appears to have a milder effect, here always paired with the pTau pathology. The morphological clusters 3 and 5 might be the selective products of some of these complex interactions, cluster 3 being more associated with A β loads and cluster 5 with pTau loads and could reflect molecularly distinct microglia states. Numerous microglia AD signatures, such as the disease-associated microglia [30, 44, 46], have been characterized in monogenic animal models mimicking A β pathology and were often observed in microglia surrounding A β plaques. If these signatures are fully or partially, regionally or sub-regionally recapitulated in human conditions still needs to be further characterized [15, 23, 57, 68, 84, 91]. Recently, Gerrits et al. [31] have defined by single-nuclei RNA sequencing that some signatures of microglia were selectively associated with A β (4G8), or with combined A β (4G8) and pTau (AT8) pathologies, in the occipital and occipitotemporal cortices of AD patients, but without investigating the possible impact of pSyn pathology. Our data support the idea of such a molecular microglia heterogeneity across the subfields of the hippocampus in AD and DLB. The complex pathological pattern of the human condition certainly represents a factor of divergence of microglia phenotypes between AD patients and monogenic rodent models. It calls for more multi-disciplinary and translational research before aiming for specific microglia signatures in the treatment of AD or DLB patients. However, if our comparison stands true at the scale of the brain, targeting microglia in DLB might be as promising as in AD.

Conclusion

Our analysis suggests that the co-occurrence of the three pTau, A β and pSyn pathologies is frequent in the hippocampus of AD and DLB patients but with a severity largely increased in AD cases. Each pathology, pTau, A β and pSyn, seems to follow a specific subregional pattern, mainly conserved across AD and DLB. Combinations and severity of subregional misfolded proteins pathologies in the hippocampus transform the local microglia phenotypic composition. The high burdens of pTau and pSyn associated with increased microglial alterations could exacerbate the CA1 vulnerability in AD.

Abbreviations

A β : Amyloid- β ; AD: Alzheimer's disease; APP: Amyloid precursor protein; CA: *Cornu ammonis*; CTL: Control; DG: *Gyrus dentatus*; DLB: Dementia with Lewy Bodies; MIC-MAC: Microglia and immune cells morphologies analyser and classifier; NFTs: Neurofibrillary tangles; PMD: Post-mortem delay; pSyn: Phosphorylated α -synuclein; pTau: Hyperphosphorylated tau; UMAP: Uniform manifold approximation and projection.

Supplementary Information

The online version contains supplementary material available at <https://doi.org/10.1186/s40478-022-01342-7>.

Additional file 1: Fig. S1. Hippocampal subfields. Anatomically defined CA1, CA3 and DG/CA4 subfields of the hippocampus for pTau, A β , pSyn and Iba1 z-stack acquisitions. Hippocampal section of an 83-year-old female AD patient (case 24) with A β (4G8, green) and microglia (Iba1, magenta) stainings. Scale bar = 1000 μ m

Additional file 2: Fig. S2. Iba1 density in hippocampal subfields of AD and DLB do not differ from age-matched CTLs. Iba1 volume (%) across conditions and hippocampal subfields

Additional file 3: Fig. S3. List and description of all morphological features with prototypic morphologies for lowest and highest feature values. Scale bars = 20 μ m

Additional file 4: Fig. S4. Microglia morphological clusters are defined by morphological features. Projection on a UMAP where each of the 32,447 individual microglia is represented by a dot with distribution spectra for volume (a), compactness (b) and polarity (c). Violin plots showing the variations of volume (d), compactness (e), polarity (f), ending nodes density (g), link density (h) and mean edge length (i) in specific clusters

Additional file 5: Fig. S5. Validation of A β and pTau stainings on FFPE samples of a neuropathologically confirmed DLB case. 3 μ m thick paraffin block sections from the temporal superior median gyrus and frontal median gyrus were obtained from the same 91-year-old male DLB patient (case 20) and were stained against A β (4G8, brown) and pTau (AT8, brown) based on the DAB/HRP substrate system with hematoxylin counterstaining. The lower rows represent a zoom of the indicated region in the upper row. Scale bars upper row = 100 μ m and lower row = 50 μ m

Additional file 6: Fig. S6. Confocal stainings of pTau, A β and pSyn across conditions and hippocampal subfields. 80–100 μ m thick hippocampal sections were immunostained with the AT8 antibody against pTau (Ser202, Thr205) (cyan), the 4G8 antibody against A β (AA17-24) (magenta) and the 11A5 antibody against pSyn (Ser129) (green). The stainings show heterogeneous distribution and types of inclusions across conditions and hippocampal subregions. Scale bars = 100 μ m

Additional file 7: Fig. 7. Validation of pSyn stainings with three different antibodies on FFPE samples of a neuropathologically confirmed DLB case. 3 μ m thick paraffin block sections from the amygdala and 80–100 μ m thick sections from fixed hippocampus were obtained from the same

91-year-old male DLB patient (case 20) and were stained against pSyn using three different antibodies, namely 11A5, 81A and EP1536Y, that all three recognize the P-Ser-129 epitope. (a) Sections from paraffin blocks were stained against pSyn (11A4, 81A and EP1536Y; brown) based on the DAB/HRP substrate system. The sections were counterstained with hematoxylin. The lower rows represent a zoom of the indicated region in the upper row. (b) Thick sections from fixed samples were stained by immunofluorescence against pSyn (11A4, 81A and EP1536Y; green), neurofilaments (NF-H, magenta) and all nuclei (DRAQ7TM, blue). Scale bars in (a) upper row = 500 μ m and lower row = 50 μ m; (b) upper row = 100 μ m and lower row = 10 μ m

Additional file 8: Fig. 8. Confocal description of pSyn staining in a neuropathologically confirmed AD case. 80–100 μ m thick sections from fixed hippocampus from a 90-year-old male AD patient (case 28) were immunostained against pSyn (11A5, 81A; green), neurofilaments (NF-H, magenta) and all nuclei (DRAQ7, blue). The upper row shows the hippocampus (stratum oriens at left bottom corner), and the lower row represents a zoom of the marked areas in the pyramidal layer. pSyn inclusions are present under various forms, including PHF-like (full triangle), Lewy neurite (empty triangle) and vacuolar aggregations (arrowhead). Scale bars upper row = 50 μ m and lower row = 20 μ m

Acknowledgements

The authors thank the Douglas Bell Canada Brain Bank and its staff for providing human brain samples, the Bioimaging Platform (BiP) of the Luxembourg Centre for Systems Biomedicine (LCSB) for support of microscopy, and the Responsible and Reproducible Research (R3) team of the LCSB for promoting reproducible research. The 11A5 antibody was kindly provided by Dr. Manuel Buttini and Dr. Wagner Zago (Prothena Biosciences).

Authors' contributions

DSB conceived and supervised the study. SF produced IHC on fixed tissue, SF and DSB performed confocal microscopy acquisitions and volumetric analysis. CA designed MIC-MAC 2.0, with inputs from SF, LS and DSB for validations. CA and GH produced statistical data analysis. OUH, CS and JJG produced some support experiments. NM provided human fixed samples. MM provided FFPE samples and resources. AS provided bioinformatic resources. SF, CA and GH produced figures. SF, CA, MM and DSB wrote the manuscript. All authors contributed to the final version of the manuscript.

Funding

This work was supported by the Espoir-en-tête Rotary International awards, the Auguste et Simone Prévot foundation and the Agaajani family donation for Alzheimer's Disease research (to DSB) and the Luxembourg National Research Fund (FNR: PEARL P16/BM/11192868 Grant) (to MM). SF and CA were supported by the PRIDE program of the Luxembourg National Research Fund through the Grants PRIDE17/12244779/PARK-QC and PRIDE17/12252781/DRIVEN respectively.

Availability of data and materials

Source code and raw data are available on <https://doi.org/10.17881/w2d6-4934>.

Declarations

Ethics approval and content to participate

All experiments involving human tissues were conducted in accordance with the guidelines approved by the Ethics Board of the Douglas Bell Canada Brain Bank (Douglas Mental Health University Institute, Montréal, QC, Canada) and the Ethic Panel of the University of Luxembourg (ERP 16-037 and 21-009). All pseudonymized autopsy brain samples were provided by the Douglas Bell Canada Brain Bank and the Luxembourg Brain Bank.

Consent for publication

Not applicable.

Competing interests

The authors report no competing interests.

Author details

¹Luxembourg Centre for Systems Biomedicine (LCSB), University of Luxembourg, Belval, Luxembourg. ²Luxembourg Center of Neuropathology (LCNP), Dudelange, Luxembourg. ³Laboratoire National de Santé (LNS), National Center of Pathology (NCP), Dudelange, Luxembourg. ⁴Swiss Data Science Center, ETH Zürich, Zürich, Switzerland. ⁵Department of Psychiatry, Douglas Mental Health University Institute, McGill University, Montreal, QC, Canada. ⁶Department of Oncology (DONC), Luxembourg Institute of Health (LIH), Strassen, Luxembourg. ⁷Department of Life Sciences and Medicine (DLSM), University of Luxembourg, Esch-sur-Alzette, Luxembourg. ⁸Faculty of Science, Technology and Medicine (FSTM), University of Luxembourg, Esch-sur-Alzette, Luxembourg.

Received: 28 February 2022 Accepted: 2 March 2022

Published online: 16 March 2022

References

- Adler DH, Wisse LEM, Ittyerah R, Pluta JB, Ding SL, Xie L, Wang J, Kadivar S, Robinson JL, Schuck T, Trojanowski JQ, Grossman M, Detre JA, Elliott MA, Toledo JB, Liu W, Pickup S, Miller MI, Das SR, Wolk DA, Yushkevich PA (2018) Characterizing the human hippocampus in aging and Alzheimer's disease using a computational atlas derived from ex vivo MRI and histology. *Proc Natl Acad Sci USA*. <https://doi.org/10.1073/pnas.1801093115>
- Amin J, Holmes C, Dorey RB, Tommasino E, Casal YR, Williams DM, Dupuy C, Nicoll JAR, Boche D (2020) Neuroinflammation in dementia with Lewy bodies: a human post-mortem study. *Transl Psychiatry*. <https://doi.org/10.1038/s41398-020-00954-8>
- Apostolova LG, Mosconi L, Thompson PM, Green AE, Hwang KS, Ramirez A, Mistur R, Tsui WH, de Leon MJ (2010) Subregional hippocampal atrophy predicts Alzheimer's dementia in the cognitively normal. *Neurobiol Aging*. <https://doi.org/10.1016/j.neurobiolaging.2008.08.008>
- Armstrong RA, Cairns NJ (2015) Comparative quantitative study of 'signature' pathological lesions in the hippocampus and adjacent gyri of 12 neurodegenerative disorders. *J Neural Transm* 122:1355–1367. <https://doi.org/10.1007/s00702-015-1402-8>
- Ayhan F, Kulkarni A, Berto S, Sivaprakasam K, Douglas C, Lega BC, Konopka G (2021) Resolving cellular and molecular diversity along the hippocampal anterior-to-posterior axis in humans. *Neuron* 109:2091–2105.e6. <https://doi.org/10.1016/j.neuron.2021.05.003>
- Bachstetter AD, Eldik LJV, Schmitt FA, Neltner JH, Ighodaro ET, Webster SJ, Patel E, Abner EL, Kryscio RJ, Nelson PT (2015) Disease-related microglia heterogeneity in the hippocampus of Alzheimer's disease, dementia with Lewy bodies, and hippocampal sclerosis of aging. *Acta Neuropathol Commun* 3:32. <https://doi.org/10.1186/s40478-015-0209-z>
- Badanjak K, Fixemer S, Smajić S, Skupin A, Grünewald A (2021) The contribution of microglia to neuroinflammation in Parkinson's disease. *IJMS* 22:4676. <https://doi.org/10.3390/ijms22094676>
- Basu J, Siegelbaum SA (2015) The corticohippocampal circuit, synaptic plasticity, and memory. *Cold Spring Harb Perspect Biol* 7:a021733. <https://doi.org/10.1101/cshperspect.a021733>
- Bird CM, Burgess N (2008) The hippocampus and memory: insights from spatial processing. *Nat Rev Neurosci* 9:182–194. <https://doi.org/10.1038/nrn2335>
- Bouvier DS, Jones EV, Quesseveur G, Davoli MA, Ferreira T, Quirion R, Mechawar N, Murai KK (2016) High resolution dissection of reactive glial nets in Alzheimer's disease. *Sci Rep* 6:24544. <https://doi.org/10.1038/srep24544>
- Braak H, Alafuzoff I, Arzberger T, Kretschmar H, Tredici K (2006) Staging of Alzheimer disease-associated neurofibrillary pathology using paraffin sections and immunocytochemistry. *Acta Neuropathol* 112:389–404. <https://doi.org/10.1007/s00401-006-0127-z>
- Braak H, Braak E (1991) Neuropathological staging of Alzheimer-related changes. *Acta Neuropathol* 82:239–259. <https://doi.org/10.1007/BF00308809>
- Burgess N, Maguire EA, O'Keefe J (2002) The human hippocampus and spatial and episodic memory. *Neuron* 35:625–641. [https://doi.org/10.1016/S0896-6273\(02\)00830-9](https://doi.org/10.1016/S0896-6273(02)00830-9)
- Candlish M, Hefendehl JK (2021) Microglia phenotypes converge in aging and neurodegenerative disease. *Front Neurol* 12:660720. <https://doi.org/10.3389/fneur.2021.660720>
- Chen WT, Lu A, Craessaerts K, Pavie B, Frigerio CS, Corthout N, Qian X, Laláková J, Kühnemund M, Voytyuk I, Wolfs L, Mancuso R, Salta E, Balusu S, Snellinx A, Munck S, Jurek A, Navarro JF, Saido TC, Huitinga I, Lundberg J, Fiers M, Strooper BD (2020) Spatial transcriptomics and in situ sequencing to study Alzheimer's disease. *Cell* 182:976–991.e19. <https://doi.org/10.1016/j.cell.2020.06.038>
- Chia R, Sabir MS, Bandres-Ciga S, Saez-Atienzar S, Reynolds RH, Gustavsson E, Walton RL, Ahmed S, Viollet C, Ding J, Makarios MB, Diez-Fairen M, Portley MK, Shah Z, Abramzon Y, Hernandez DG, Blauwendraat C, Stone DJ, Eicher J, Parkkinen L, Ansorge O, Clark L, Honig LS, Marder K, Lemstra A, George-Hyslop PS, Londos E, Morgan K, Lashley T, Warner TT, Jaunmuktane Z, Galasko D, Santana I, Tienari PJ, Myllykangas L, Oinas M, Cairns NJ, Morris JC, Halliday GM, Deerlin VMV, Trojanowski JQ, Grassano M, Calvo A, Mora G, Canosa A, Floris G, Bohannan RC, Brett F, Gan-Or Z, Geiger JT, Moore A, May P, Krüger R, Goldstein DS, Lopez G, Tayebi N, Sidransky E, Sotis AR, Sukumar G, Alba C, Lott N, Martinez EMG, Tuck M, Singh J, Bacikova D, Zhang X, Hupalo DN, Adeleye A, Wilkerson MD, Pollard HB, Norcliffe-Kaufmann L, Palma JA, Kaufmann H, Shakkottai VG, Perkins M, Newell KL, Gasser T, Schulte C, Landi F, Salvi E, Cusi D, Masliah E, Kim RC, Caraway CA, Monuki ES, Brunetti M, Dawson TM, Rosenthal LS, Albert MS, Pletnikova O, Troncoso JC, Flanagan ME, Mao Q, Bigio EH, Rodríguez-Rodríguez E, Infante J, Lage C, González-Aramburu I, Sanchez-Juan P, Ghetti B, Keith J, Black SE, Masellis M, Rogaeva E, Duyckaerts C, Brice A, Lesage S, Xiomerisiou G, Barrett MJ, Tilley BS, Gentleman S, Logroscino G, Serrano GE, Beach TG, McKeith IG, Thomas AJ, Attems J, Morris CM, Palmer L, Love S, Troakes C, Al-Sarraj S, Hodges AK, Aarsland D, Klein G, Kaiser SM, Woltjer R, Pastor P, Bekris LM, Leverenz JB, Besser LM, Kuzma A, Renton AE, Goate A, Bennett DA, Scherzer CR, Morris HR, Ferrari R, Albani D, Pickering-Brown S, Faber K, Kukull WA, Morenas-Rodríguez E, Lleó A, Fortea J, Alcolea D, Clarimon J, Nalls MA, Ferrucci L, Resnick SM, Tanaka T, Frouad TM, Graff-Radford NR, Wszolek ZK, Ferman T, Boeve BF, Hardy JA, Topol EJ, Torkamani A, Singleton AB, Ryten M, Dickson DW, Chiò A, Ross OA, Gibbs JR, Dalgard CL, Traynor BJ, Scholz SW (2021) Genome sequencing analysis identifies new loci associated with Lewy body dementia and provides insights into its genetic architecture. *Nat Genet* 53:294–303. <https://doi.org/10.1038/s41588-021-00785-3>
- Colom-Cadena M, Gelpi E, Charif S, Belbin O, Blesa R, Martí MJ, Clarimón J, Lleó A (2013) Confluence of α -synuclein, tau, and β -amyloid pathologies in dementia with Lewy bodies. *J Neuropathol Exp Neurol* 72:1203–1212. <https://doi.org/10.1097/NEN.0000000000000018>
- Coras R, Pauli E, Li J, Schwarz M, Rössler K, Buchfelder M, Hamer H, Stefan H, Blumcke I (2014) Differential influence of hippocampal subfields to memory formation: insights from patients with temporal lobe epilepsy. *Brain*. <https://doi.org/10.1093/brain/awu100>
- Coughlin DG, Ittyerah R, Peterson C, Phillips JS, Miller S, Rascovsky K, Weintraub D, Siderowf AD, Duda JE, Hurtig HI, Wolk DA, McMillan CT, Yushkevich PA, Grossman M, Lee EB, Trojanowski JQ, Irwin DJ (2020) Hippocampal subfield pathologic burden in Lewy body diseases vs. Alzheimer's disease. *Neuropathol Appl Neurobiol*. <https://doi.org/10.1111/nan.12659>
- Crist AM, Hinkle KM, Wang X, Moloney CM, Matchett BJ, Labuzan SA, Frankenhauser I, Azu NO, Liesinger AM, Lesser ER, Serie DJ, Quicksall ZS, Patel TA, Carnwath TP, DeTure M, Tang X, Petersen RC, Duara R, Graff-Radford NR, Allen M, Carrasquillo MM, Li H, Ross OA, Ertekin-Taner N, Dickson DW, Asmann YW, Carter RE, Murray ME (2021) Transcriptomic analysis to identify genes associated with selective hippocampal vulnerability in Alzheimer's disease. *Nat Commun*. <https://doi.org/10.1038/s41467-021-22399-3>
- Crystal H, Dickson D, Fuld P, Masur D, Scott R, Mehler M, Masdeu J, Kawas C, Aronson M, Wolfson L (1988) Clinico-pathologic studies in dementia: Nondemented subjects with pathologically confirmed Alzheimer's disease. *Neurology*. <https://doi.org/10.1212/wnl.38.11.1682>
- Dabov K, Foi A, Katkovnik V, Egiazarian K (2008) Image restoration by sparse 3D transform-domain collaborative filtering. In: *Proceedings volume 6812, image processing: algorithms and systems VI*
- Del-Aguila JL, Li Z, Dube U, Mihindukulasuriya KA, Budde JP, Fernandez MV, Ibanez L, Bradley J, Wang F, Bergmann K, Davenport R, Morris JC, Holtzman DM, Perrin RJ, Benitez BA, Dougherty J, Cruchaga C, Harari O

- (2019) A single-nuclei RNA sequencing study of Mendelian and sporadic AD in the human brain. *Alzheimer's Res Ther*. <https://doi.org/10.1186/s13195-019-0524-x>
24. Dubois B (2018) The emergence of a new conceptual framework for Alzheimer's disease. *J Alzheimer's Dis* 62:1059–1066. <https://doi.org/10.3233/JAD-170536>
 25. Femminella GD, Ninan S, Atkinson R, Fan Z, Brooks DJ, Edison P (2016) Does microglial activation influence hippocampal volume and neuronal function in Alzheimer's disease and Parkinson's disease dementia? *J Alzheimer's Dis* 51:1275–1289. <https://doi.org/10.3233/JAD-150827>
 26. Ferrarini L, Lew BV, Reiber JHC, Gandin C, Galluzzo L, Scafato E, Frisoni GB, Milles J, Pievani M, Farchi G, Giampaoli S, Mariotti S, Gandin C, Galluzzo L, Ghirini S, Martire S, Pasquale LD, Maggi S, Crepaldi G, Enzi G, Gallina P, Inzitari D, Baldereschi M, Carlo AD, Galluzzi S, Gandolfo C, Conti M, Postacchini D, Cruciani G, Giuli C, Capurso A, Solfrizzi V, Panza F, Rengo F, Abete P, Motta M, Negrini R, Forti P, Tabanelli P, Cocchi A, Zuccal G, Cacciatore F, Calabrese C, Sica G, Estraneo A, Consoli D, Naso F, Torcasio G, Mecocci P, Rinaldi P, Serafini V, Senin U (2014) Hippocampal atrophy in people with memory deficits: results from the population-based IPREA study. *Int Psychogeriatr*. <https://doi.org/10.1017/S1041610213002627>
 27. Ferreira D, Przybelski SA, Lesnick TG, Lemstra AW, Londos E, Blanc F, Nedelska Z, Schwarz CG, Graff-Radford J, Senjem ML, Fields JA, Knopman DS, Savica R, Ferman TJ, Graff-Radford NR, Lowe VJ, Jack CR, Petersen RC, Mollenhauer B, Garcia-Ptacek S, Abdelnour C, Hort J, Bonanni L, Oppedal K, Kramberger MG, Boeve BF, Aarsland D, Westman E, Kantarci K (2020) β -Amyloid and tau biomarkers and clinical phenotype in dementia with Lewy bodies. *Neurology*. <https://doi.org/10.1212/WNL.00000000001010943>
 28. Foo H, Thalamuthu A, Jiang J, Koch F, Mather KA, Wen W, Sachdev PS (2021) Associations between Alzheimer's disease polygenic risk scores and hippocampal subfield volumes in 17,161 UK Biobank participants. *Neurobiol Aging* 98:108–115. <https://doi.org/10.1016/j.neurobiolaging.2020.11.002>
 29. Freund Y, Schapire RE (1997) A decision-theoretic generalization of on-line learning and an application to boosting. *J Comput Syst Sci*. <https://doi.org/10.1006/jcss.1997.1504>
 30. Frigerio CS, Wolfs L, Fattorelli N, Thrupp N, Voytyuk I, Schmidt I, Mancuso R, Chen WT, Woodbury ME, Srivastava G, Möller T, Hudry E, Das S, Saito T, Karran E, Hyman B, Perry VH, Fiers M, Strooper BD (2019) The major risk factors for Alzheimer's disease: age, sex, and genes modulate the microglia response to A β plaques. *Cell Rep*. <https://doi.org/10.1016/j.celrep.2019.03.099>
 31. Gerrits E, Brouwer N, Kooistra SM, Woodbury ME, Vermeiren Y, Lambourne M, Mulder J, Kummer M, Möller T, Biber K, den Dunnen WFA, Deyn PPD, Eggen BJL, Boddeke EWGM (2021) Distinct amyloid- β and tau-associated microglia profiles in Alzheimer's disease. *Acta Neuropathol* 141:681–696. <https://doi.org/10.1007/s00401-021-02263-w>
 32. Goedert M, Jakes R, Vanmechelen E (1995) Monoclonal antibody AT8 recognises tau protein phosphorylated at both serine 202 and threonine 205. *Neurosci Lett* 189:167–170. [https://doi.org/10.1016/0304-3940\(95\)11484-E](https://doi.org/10.1016/0304-3940(95)11484-E)
 33. Golde TE, Borchelt DR, Giasson BI, Lewis J (2013) Thinking laterally about neurodegenerative proteinopathies. *J Clin Investig*. <https://doi.org/10.1172/JCI66029>
 34. Golomb J, Leon MJ, Kluger A, Tarshish C, Ferris SH, George AE (1993) Hippocampal atrophy in normal aging: an association with recent memory impairment. *Arch Neurol*. <https://doi.org/10.1001/archneur.1993.00540090066012>
 35. Griffin WST, Liu L, Li Y, Mrak RE, Barger SW (2006) Interleukin-1 mediates Alzheimer and Lewy body pathologies. *J Neuroinflamm* 3:1–9. <https://doi.org/10.1186/1742-2094-3-5>
 36. Grubman A, Choo XY, Chew G, Ouyang JF, Sun G, Croft NP, Rossello FJ, Simmons R, Buckberry S, Landin DV, Pflueger J, Vandekolk TH, Abay Z, Zhou Y, Liu X, Chen J, Larcombe M, Haynes JM, McLean C, Williams S, Chai SY, Wilson T, Lister R, Pouton CW, Purcell AW, Rackham OJL, Petretto E, Polo JM (2021) Transcriptional signature in microglia associated with A β plaque phagocytosis. *Nat Commun*. <https://doi.org/10.1038/s41467-021-23111-1>
 37. Hunter S, Brayne C (2017) Do anti-amyloid beta protein antibody cross reactivities confound Alzheimer disease research? *J Negat Res Biomed* 16:1–8. <https://doi.org/10.1186/s12952-017-0066-3>
 38. Iseki E, Takayama N, Marui W, Ueda K, Kosaka K (2002) Relationship in the formation process between neurofibrillary tangles and Lewy bodies in the hippocampus of dementia with Lewy bodies brains. *J Neurol Sci* 195:85–91. [https://doi.org/10.1016/S0022-510X\(01\)00689-X](https://doi.org/10.1016/S0022-510X(01)00689-X)
 39. Jansen WJ, Ossenkuppele R, Knol DL, Tijms BM, Scheltens P, Verhey FRJ, Visser PJ, Aalten P, Aarsland D, Alcolea D, Alexander M, Almdahl IS, Arnold SE, Baldeiras I, Barthel H, Berckel BNMV, Bibeau K, Blennow K, Brooks DJ, Buchem MAV, Camus V, Cavedo E, Chen K, Chételat G, Cohen AD, Drzezga A, Engelborghs S, Fagan AM, Fladby T, Fleisher AS, Flier WMVD, Ford L, Forster S, Fortea J, Fosskett N, Frederiksen KS, Freund-Levi Y, Frisoni GB, Froelich L, Gabryelewicz T, Gill KD, Gkatzima O, Gomez-Tortosa E, Gordon MF, Grimmer T, Hampel H, Hausner L, Hellwig S, Herukka SK, Hildebrandt H, Ishihara L, Ivanoiu A, Jagust WJ, Johannsen P, Kandimalla R, Kapaki E, Klimkowicz-Mrowiec A, Klunk WE, Kohler S, Koglin N, Kornhuber J, Kramberger MG, Laere KV, Landau SM, Lee DY, Leon MD, Lisetti V, Lleo A, Madsen K, Maier W, Marcusson J, Mattsson N, Mendonca AD, Meulenberg O, Meyer PT, Mintun MA, Mok V, Molinuevo JL, Mollergard HM, Morris JC, Mroczko B, Mussele SVD, Na DL, Newberg A, Nordberg A, Nordlund A, Novak GP, Paraskevas GP, Parnetti L, Perera G, Peters O, Popp J, Prabhakar S, Rabinovici GD, Ramakers IHGB, Rami L, Oliveira CRD, Rinne JO, Rodrigue KM, Rodriguez-Rodriguez E, Roe CM, Rot U, Rowe CC, Ruther E, Sabri O, Sanchez-Juan P, Santana I, Sarazin M, Schroder J, Schutte C, Seo SW, Soetewey F, Sooinen H, Spuru L, Struys H, Teunissen CE, Tsolaki M, Vandenbergh R, Verbeek MM, Villemagne VL, Vos SJB, Doorn LJCWVW, Waldemar G, Wallin A, Wallin AK, Wiltfang J, Wolk DA, Zboch M, Zetterberg H (2015) Prevalence of cerebral amyloid pathology in persons without dementia: a meta-analysis. *JAMA J Am Med Assoc*. <https://doi.org/10.1001/jama.2015.4668>
 40. Joie RL, Perrotin A, Sayette VDL, Egret S, Doeuvre L, Belliard S, Eustache F, Desgranges B, Chételat G (2013) Hippocampal subfield volumetry in mild cognitive impairment, Alzheimer's disease and semantic dementia. *NeuroImage Clin*. <https://doi.org/10.1016/j.nicl.2013.08.007>
 41. Josephs KA, Dickson DW, Tosakulwong N, Weigand SD, Murray ME, Petrucelli L, Liesinger AM, Senjem ML, Spychalla AJ, Knopman DS, Parisi JE, Petersen RC, Jack CR, Whitwell JL (2017) Rates of hippocampal atrophy and presence of post-mortem TDP-43 in patients with Alzheimer's disease: a longitudinal retrospective study. *Lancet Neurol* 16:917–924. [https://doi.org/10.1016/S1474-4422\(17\)30284-3](https://doi.org/10.1016/S1474-4422(17)30284-3)
 42. Kawas CH, Kim RC, Sonnen JA, Bullain SS, Trieu C, Corrada MM (2015) Multiple pathologies are common and related to dementia in the oldest-old: the 90+ Study. *Neurology*. <https://doi.org/10.1212/WNL.000000000001831>
 43. Kerchner GA, Deutsch GK, Zeineh M, Dougherty RF, Saranathan M, Rutt BK (2012) Hippocampal CA1 apical neuropil atrophy and memory performance in Alzheimer's disease. *Neuroimage*. <https://doi.org/10.1016/j.neuroimage.2012.06.048>
 44. Keren-Shaul H, Spinrad A, Weiner A, Matcovitch-Natan O, Dvir-Szternfeld R, Ulland TK, David E, Baruch K, Lara-Astaiso D, Toth B, Itzkovitz S, Colonna M, Schwartz M, Amit I (2017) A unique microglia type associated with restricting development of Alzheimer's disease. *Cell* 169:1276–1290.e17. <https://doi.org/10.1016/j.cell.2017.05.018>
 45. Kovacs GG, Milenkovic I, Wöhler A, Höftberger R, Gelpi E, Haberler C, Hönigschnabl S, Reiner-Concin A, Heinzl H, Jungwirth S, Krampla W, Fischer P, Budka H (2013) Non-Alzheimer neurodegenerative pathologies and their combinations are more frequent than commonly believed in the elderly brain: a community-based autopsy series. *Acta Neuropathol*. <https://doi.org/10.1007/s00401-013-1157-y>
 46. Krasemann S, Madore C, Cialic R, Baufeld C, Calcagno N, Fatimy RE, Beckers L, O'Loughlin E, Xu Y, Fanek Z, Greco DJ, Smith ST, Tsvet G, Humulock Z, Zrzavy T, Conde-Sanroman P, Gacias M, Weng Z, Chen H, Tjon E, Mazaheri F, Hartmann K, Madi A, Ulrich JD, Glatzel M, Worthmann A, Heeren J, Budnik B, Lemere C, Ikezu T, Heppner FL, Litvak V, Holtzman DM, Lassmann H, Weiner HL, Ochando J, Haass C, Butovsky O (2017) The TREM2-APOE pathway drives the transcriptional phenotype of dysfunctional microglia in neurodegenerative diseases. *Immunity*. <https://doi.org/10.1016/j.immuni.2017.08.008>
 47. Lashuel HA (2021) Rethinking protein aggregation and drug discovery in neurodegenerative diseases: why we need to embrace complexity? *Curr Opin Chem Biol* 64:67–75. <https://doi.org/10.1016/J.CBPA.2021.05.006>

48. Lee CYD, Landreth GE (2010) The role of microglia in amyloid clearance from the AD brain. *J Neural Transm* 117:949–960. <https://doi.org/10.1007/s00702-010-0433-4>
49. Lisman J, Redish AD (2018) Viewpoints: how the hippocampus contributes to memory, navigation and cognition. *Nat Neurosci* 20:1434–1447. <https://doi.org/10.1038/nn.4661>
50. Lucy LB (1974) An iterative technique for the rectification of observed distributions. *Astron J*. <https://doi.org/10.1086/111605>
51. Luo W, Liu W, Hu X, Hanna M, Caravaca A, Paul SM (2015) Microglial internalization and degradation of pathological tau is enhanced by an anti-tau monoclonal antibody. *Sci Rep*. <https://doi.org/10.1038/srep11161>
52. Mackenzie IRA (2000) Activated microglia in dementia with Lewy bodies. *Neurology* 55:132–134. <https://doi.org/10.1212/WNL.55.1.132>
53. Mak E, Su L, Williams GB, Watson R, Firbank M, Blamire A, O'Brien J (2016) Differential atrophy of hippocampal subfields: a comparative study of dementia with lewy bodies and Alzheimer disease. *Am J Geriatric Psychiatry* 24:136–143. <https://doi.org/10.1016/j.jagp.2015.06.006>
54. Markesbery WR, Jicha GA, Liu H, Schmitt FA (2009) Lewy body pathology in normal elderly subjects. *J Neuropathol Exp Neurol*. <https://doi.org/10.1097/NEN.0b013e3181ac10a7>
55. Márquez-Ropero M, Benito E, Plaza-Zabala A, Sierra A (2020) Microglial corpse clearance: lessons from macrophages. *Front Immunol* 11:506. <https://doi.org/10.3389/fimmu.2020.00506>
56. Masuda T, Sankowski R, Staszewski O, Böttcher C, Amann L, Sagar SC, Nessler S, Kunz P, van Loo G, Coenen VA, Reinacher PC, Michel A, Sure U, Gold R, Grün D, Priller J, Stadelmann C, Prinz M (2019) Spatial and temporal heterogeneity of mouse and human microglia at single-cell resolution. *Nature* 566:388–392. <https://doi.org/10.1038/s41586-019-0924-x>
57. Mathys H, Davila-Velderrain J, Peng Z, Gao F, Mohammadi S, Young JZ, Menon M, He L, Abdurrob F, Jiang X, Martorell AJ, Ransohoff RM, Hafler BP, Bennett DA, Kellis M, Tsai LH (2019) Single-cell transcriptomic analysis of Alzheimer's disease. *Nature*. <https://doi.org/10.1038/s41586-019-1195-2>
58. McInnes L, Healy J, Saul N, Großberger L (2018) UMAP: uniform manifold approximation and projection. *J Open Source Softw*. <https://doi.org/10.21105/joss.00861>
59. McKeith IG (2006) Consensus guidelines for the clinical and pathologic diagnosis of dementia with Lewy bodies (DLB): report of the consortium on DLB international workshop. *JAD* 9:417–423. <https://doi.org/10.3233/JAD-2006-95347>
60. Boeve MIGDD, BF, (2017) Diagnosis and management of dementia with Lewy bodies: fourth consensus report of the DLB Consortium. *Neurology*. <https://doi.org/10.1212/WNL.0000000000004058>
61. McQuade A, Blurton-Jones M (2019) Microglia in Alzheimer's disease: exploring how genetics and phenotype influence risk. *J Mol Biol* 431:1805–1817. <https://doi.org/10.1016/j.jmb.2019.01.045>
62. Meneses A, Koga S, Leary JO, Dickson DW, Bu G, Zhao N (2021) TDP-43 pathology in Alzheimer's disease. *Mol Neurodegener* 16(84):1–15. <https://doi.org/10.1186/s13024-021-00503-x>
63. Montine TJ, Phelps CH, Beach TG, Bigio EH, Cairns NJ, Dickson DW, Duyckaerts C, Frosch MP, Masliah E, Mirra SS, Nelson PT, Schneider JA, Thal DR, Trojanowski JQ, Vinters HV, Hyman BT (2012) National institute on aging-Alzheimer's association guidelines for the neuropathologic assessment of Alzheimer's disease: a practical approach. *Acta Neuropathol*. <https://doi.org/10.1007/s00401-011-0910-3>
64. Mrdjen D, Fox EJ, Bukhari SA, Montine KS, Bendall SC, Montine TJ (2019) The basis of cellular and regional vulnerability in Alzheimer's disease. *Acta Neuropathol* 138:729–749. <https://doi.org/10.1007/s00401-019-02054-4>
65. Nakashima-Yasuda H, Uryu K, Robinson J, Xie SX, Hurtig H, Duda JE, Arnold SE, Siderowf A, Grossman M, Leverenz JB, Woltjer R, Lopez OL, Hamilton R, Tsuang DW, Galasko D, Masliah E, Kaye J, Clark CM, Montine TJ, Lee VM-Y, Trojanowski JQ (2007) Co-morbidity of TDP-43 proteinopathy in Lewy body related diseases. *Acta Neuropathol* 114:221–229. <https://doi.org/10.1007/s00401-007-0261-2>
66. Paasila PJ, Davies DS, Kril JJ, Goldsberry C, Sutherland GT (2019) The relationship between the morphological subtypes of microglia and Alzheimer's disease neuropathology. *Brain Pathol*. <https://doi.org/10.1111/bpa.12717>
67. Paoilicelli RC, Jawaid A, Henstridge CM, Valeri A, Merlini M, Robinson JL, Lee EB, Rose J, Appel S, Lee VMY, Trojanowski JQ, Spires-Jones T, Schulz PE, Rajendran L (2017) TDP-43 depletion in microglia promotes amyloid clearance but also induces synapse loss. *Neuron* 95:297–308.e6. <https://doi.org/10.1016/j.neuron.2017.05.037>
68. Patir A, Shih B, McColl BW, Freeman TC (2019) A core transcriptional signature of human microglia: derivation and utility in describing region-dependent alterations associated with Alzheimer's disease. *Glia* 67:1240–1253. <https://doi.org/10.1002/glia.23572>
69. Prinz M, Jung S, Priller J (2019) Microglia biology: one century of evolving concepts. *Cell* 179:292–311. <https://doi.org/10.1016/j.cell.2019.08.053>
70. Quesseveur G, Fouquier d'Hérouël A, Murai KK, Bouvier DS (2019) A specialized method to resolve fine 3D features of astrocytes in nonhuman primate (Marmoset, *Callithrix jacchus*) and human fixed brain samples. In: Di Benedetto B (ed) *Astrocytes*. Springer, New York, pp 85–95
71. Richardson WH (1972) Bayesian-based iterative method of image restoration*. *J Opt Soc Am*. <https://doi.org/10.1364/josa.62.000055>
72. Robinson JL, Lee EB, Xie SX, Rennett L, Suh E, Bredenberg C, Caswell C, Deerlin VMV, Yan N, Yousef A, Hurtig HI, Siderowf A, Grossman M, McMillan CT, Miller B, Duda JE, Irwin DJ, Wolk D, Elman L, McCluskey L, Chen-Plotkin A, Weintraub D, Arnold SE, Brettschneider J, Lee VMY, Trojanowski JQ (2018) Neurodegenerative disease concomitant proteinopathies are prevalent, age-related and APOE4-associated. *Brain*. <https://doi.org/10.1093/brain/awy146>
73. Rodrigue KM, Kennedy KM, Devous MD, Rieck JR, Hebrank AC, Diaz-Arrastia R, Mathews D, Park DC (2012) β -amyloid burden in healthy aging: regional distribution and cognitive consequences. *Neurology*. <https://doi.org/10.1212/WNL.0b013e318245d295>
74. Sabatelli F, Boccardi M, Galluzzi S, Treves A, Thompson PM, Frisoni GB (2008) Hippocampal shape differences in dementia with Lewy bodies. *Neuroimage*. <https://doi.org/10.1016/j.neuroimage.2008.02.060>
75. Salamanca L, Mechawar N, Murai KK, Balling R, Bouvier DS, Skupin A (2019) MIC-MAC: An automated pipeline for high-throughput characterization and classification of three-dimensional microglia morphologies in mouse and human postmortem brain samples. *Glia*. <https://doi.org/10.1002/glia.23623>
76. Salter MW, Stevens B (2017) Microglia emerge as central players in brain disease. *Nat Med* 23:1018–1027. <https://doi.org/10.1038/nm.4397>
77. Sanchez-Mejias E, Navarro V, Jimenez S, Sanchez-Mico M, Sanchez-Varo R, Nuñez-Diaz C, Trujillo-Estrada L, Davila JC, Vizuete M, Gutierrez A, Vitorica J (2016) Soluble phospho-tau from Alzheimer's disease hippocampus drives microglial degeneration. *Acta Neuropathol*. <https://doi.org/10.1007/s00401-016-1630-5>
78. Sarlus H, Heneka MT (2017) Microglia in Alzheimer's disease. *J Clin Invest* 127:3240–3249. <https://doi.org/10.1172/JCI90606>
79. Savage JC, Carrier M, Tremblay M-E (2019) Chapter 2 morphology of microglia across contexts of health. *Methods Mol Biol*. https://doi.org/10.1007/978-1-4939-9658-2_2
80. Schmidt ML, Martin JA, Lee VMY, Trojanowski JQ (1996) Convergence of Lewy bodies and neurofibrillary tangles in amygdala neurons of Alzheimer's disease and Lewy body disorders. *Acta Neuropathol* 91:475–481. <https://doi.org/10.1007/s004010050454>
81. Schumacher J, Gunter JL, Przybelski SA, Jones DT, Graff-Radford J, Savica R, Schwarz CG, Senjem ML, Jack CR, Lowe VJ, Knopman DS, Fields JA, Kremers WK, Petersen RC, Graff-Radford NR, Ferman TJ, Boeve BF, Thomas AJ, Taylor J-P, Kantarci K (2021) Dementia with Lewy bodies: association of Alzheimer pathology with functional connectivity networks. *Brain*. <https://doi.org/10.1093/brain/awab218>
82. Seok JW, Cheong C (2020) Functional dissociation of hippocampal subregions corresponding to memory types and stages. *J Physiol Anthropol*. <https://doi.org/10.1186/s40101-020-00225-x>
83. Španić E, Langer Horvat L, Hof PR, Šimić G (2019) Role of microglial cells in Alzheimer's disease tau propagation. *Front Aging Neurosci* 11:271. <https://doi.org/10.3389/fnagi.2019.00271>
84. Srinivasan K, Friedman BA, Etxeberria A, Huntley MA, van der Brug MP, Foreman O, Paw JS, Modrusan Z, Beach TG, Serrano GE, Hansen DV (2020) Alzheimer's patient microglia exhibit enhanced aging and unique transcriptional activation. *Cell Rep*. <https://doi.org/10.1016/j.celrep.2020.107843>
85. Strange BA, Witter MP, Lein ES, Moser EI (2014) Functional organization of the hippocampal longitudinal axis. *Nat Rev Neurosci* 15:655–669. <https://doi.org/10.1038/nrn3785>
86. Streit WJ, Xue QS (2016) Microglia in dementia with Lewy bodies. *Brain Behav Immun* 55:191–201. <https://doi.org/10.1016/j.bbi.2015.10.012>

87. Surendranathan A, Su L, Mak E, Passamonti L, Hong YT, Arnold R, Rodríguez PV, Bevan-Jones WR, Brain SAE, Fryer TD, Aigbirhio FI, Rowe JB, O'Brien JT (2018) Early microglial activation and peripheral inflammation in dementia with Lewy bodies. *Brain* 141:3415–3427. <https://doi.org/10.1093/brain/awy265>
88. Thal DR, Rüb U, Orantes M, Braak H (2002) Phases of A β -deposition in the human brain and its relevance for the development of AD. *Neurology* 58:1791–1800. <https://doi.org/10.1212/WNL.58.12.1791>
89. Tracy TE, Madero-Pérez J, Swaney DL, Chang TS, Moritz M, Konrad C, Ward ME, Stevenson E, Hüttenhain R, Kauwe G, Mercedes M, Sweetland-Martin L, Chen X, Mok S-A, Wong MY, Telpoukhovskaia M, Min S-W, Wang C, Sohn PD, Martin J, Zhou Y, Luo W, Trojanowski JQ, Lee VMY, Gong S, Manfredi G, Coppola G, Krogan NJ, Geschwind DH, Gan L (2022) Tau interactome maps synaptic and mitochondrial processes associated with neurodegeneration. *Cell* 185:712–728.e14. <https://doi.org/10.1016/j.cell.2021.12.041>
90. Uriarte Huarte O, Richart L, Mittelbronn M, Michelucci A (2021) Microglia in health and disease: the strength to be diverse and reactive. *Front Cell Neurosci* 15:660523. <https://doi.org/10.3389/fncel.2021.660523>
91. Walker DG (2020) Defining activation states of microglia in human brain tissue: an unresolved issue for Alzheimer's disease. *Neuroimmunol Neuroinflamm.* <https://doi.org/10.20517/2347-8659.2020.09>
92. Walker L, McAleese KE, Thomas AJ, Johnson M, Martin-Ruiz C, Parker C, Colloby SJ, Jellinger KA, Attems J (2015) Neuropathologically mixed Alzheimer's and Lewy body disease: burden of pathological protein aggregates differs between clinical phenotypes. *Acta Neuropathol.* <https://doi.org/10.1007/s00401-015-1406-3>
93. Ward JH (1963) Hierarchical grouping to optimize an objective function. *J Am Stat Assoc.* <https://doi.org/10.1080/01621459.1963.10500845>
94. Yassa MA, Stark CEL (2011) Pattern separation in the hippocampus. *Trends Neurosci* 34:515–525. <https://doi.org/10.1016/j.tins.2011.06.006>
95. Zeisel A, Muñoz-Manchado AB, Codeluppi S, Lönnerberg P, La Manno G, Jureus A, Marques S, Munguba H, He L, Betsholtz C, Rolny C, Castelo-Branco G, Hjerling-Leffler J, Linnarsson S (2015) Cell types in the mouse cortex and hippocampus revealed by single-cell RNA-seq. *Science* 347:1138–1142. <https://doi.org/10.1126/science.aaa1934>
96. Zhao W, Wang X, Yin C, He M, Li S, Han Y (2019) Trajectories of the hippocampal subfields atrophy in the Alzheimer's disease: a structural imaging study. *Front Neuroinform.* <https://doi.org/10.3389/fninf.2019.00013>

Publisher's Note

Springer Nature remains neutral with regard to jurisdictional claims in published maps and institutional affiliations.

Ready to submit your research? Choose BMC and benefit from:

- fast, convenient online submission
- thorough peer review by experienced researchers in your field
- rapid publication on acceptance
- support for research data, including large and complex data types
- gold Open Access which fosters wider collaboration and increased citations
- maximum visibility for your research: over 100M website views per year

At BMC, research is always in progress.

Learn more biomedcentral.com/submissions

